RESULTS FROM THE NCC/NICMOS SPARE-DETECTOR JUNE 2000 EMI TEST

A report to NASA/GSFC and STScI

Glenn Schneider (gschneider@as.arizona.edu)
Steward Observatory
University of Arizona
12 August 2000

0. SUMMARY

Analysis of power spectra and images obtained with a NICMOS-3 flight spare detector, operated in conjunction with the NICMOS Cryo-Cooler (NCC) and mated with flight-like ground connections, indicate the total absence of any NCC induced electromagnetic interference in any of the more than 3000 NICMOS science data readouts (64K pixel) images examined. As a differential experiment, making use of the independently measured time-correlated samples provided by each of the four detector quadrants, the system sensitivities to detect EMI induced periodic and quasi-periodic signals in the frequency range from 5 Hz to 50 Khz closely reached, or exceeded, the per-pixel sensitivities of the NICMOS flight detectors in the flight instrument. A similar experiment performed in May, 1998, before the NCC test on the HOST mission, revealed the presence of complex broad-band signals impressed in the NICMOS science data readouts manifesting themselves as temporally varying "herringbone" patterns in the images with strong power components in the ~ 5-9 Khz region. The June 2000 test was conducted over a period of two days with NICMOS data collected with the NCC in an "off" state, and while being operated at a variety of compressor speeds from 5000 to 7200 rps. While significant non-NCC induced 60/180Hz contamination at the 10 DN (50 electron) peak-to-peak level was prevalent, and much smaller amplitude monochromatic signals were seen at higher frequencies, these were both unquestionably due to other sources. Frames taken with the NCC on and off were indistinguishable. It is apparent that changes in the NCC design and their implementation since its pre-HOST incarnation have succeeded in producing a unit which produces no measurable levels of induced signals in NICMOS science data readouts and is fully compatible with the use of NICMOS detectors on-orbit thereby alleviating previous EMI concerns.

1. INTRODUCTION

On June 27-28, 2000, as part of the NICMOS cryo-cooler testing program, the UofA NICMOS Project (see Appendix A) in concert with GSFC and STScI conducted an experiment to ascertain the possible susceptibility of a NICMOS-3 detector to conducted and/or radiated electromagnetic interference from the NICMOS cryo-cooler. A flight-spare detector (#97T0012) on a flight mount in a UofA test dewar (HDL-8 from IR Labs), was shipped to GSFC for this investigation. All control, signal, data, and power connections were made between the test dewar and a functional replica of the NICMOS flight electronics (a "Baseline Release Zero, or BRZ rack) in an electrically flight-like configuration. Grounding and mechanical connections to the test dewar and the cryo-cooler system were also established (by Creare, GSFC and UofA personnel) to emulate flight-like conditions. Conductance measures at the ground points were made at the start of each test day after (re)-integrating the dewar with the NCC and are given in Table 1.1.

```
     Table 1.1  Ground Connection Conductances
          (resistivities in milliOhms)


                            DAY 179   DAY 180
     Cooler to Ground-Strap    2.4       2.3
     Cooler to Dewar           3.5       3.6
     Dewar to Ground-Strap     3.0       2.3
     Cooler to Wall            3.4       2.6
```

The mechanical configuration of the NCC and test dewar are shown in a series of photographs which may be downloaded from a NICMOS/UofA server at the URL:

http://nicmosis.as.arizona.edu:8000/NCC_EMI_2000/EMI_JPG/NCC_EMI_PHOTOS.html

Testing was carried out in an EMI clean/screen room at GSFC to attenuate outside interference. A series of images were obtained to map the spectral frequencies of any NCC induced EMI in NICMOS science data. Data were obtained using in-flight detector timing and clocking patterns as per normal on-orbit operations via stored command loads executing on a SITS system.

2. SAMPLING STRATEGY USING NICMOS-3 DETECTOR AND NICMOS FSW

The primary sampling strategy employed multiple 3-repeat sets of 25-read 1.2-second delta-time mutltiaccum exposures, and was identical to that used in the April 1998 test. The reader is referred to the test report "EMI Noise Properties of the NICMOS Cooling System as Seen by a NICMOS-3 Flight Spare Detector" (G. Schneider, UofA, 1 May 1998) for both background and more detailed information. In addition, two other multiaccum timing patterns were used at the request of STScI. The first employed asynchronous delta-times between reads, and the second a standard STEP64 readout pattern commonly used on-orbit. In this report, other than a first quick-look at the asynchronouly sampled data, we discuss only the results derived from the 26-read 1.2-second delta-time multiaccums.

3. DATA COLLECTION, FORMAT and DISTRIBUTION

The NICMOS spare detector data, obtained with the GSFC VEST/BRZ system in the EMI test environment and which were the basis of this report, were delivered to STScI for independent verification of our findings. Those data, originally processed through the SI C&DH/SDF model in the SITS system were acquired as POD (.SDI) files and converted to FITS format with GENCONVERT (a rough analog to a subset of the generic conversion routines running in the OPUS environment). Those files were reformatted in post-processing to conform to the multiple science extension "multiaccum" format used for NICMOS science data delivered to observers by STScI and archived in the HDA, though we have written only science (SCI) extensions. In compliance with the multiaccum data file format defined by STScI, the science extensions are written in inverse time order, so that read 0 (the first readout after completing the detector reset cycle, also called the bias read) is the last science extension in the file. The data are treated as "raw", and hence uncalibrated, and are written as signed 16-bit integers. Each science extension is documented with FITS header keyword/value pairs which capture the exposure and readout information (in the EXPOSURE INFORMATION and READOUT PARAMETERS sections) of particular necessity to this test.

Engineering telemetry capturing the state of the NCC was collected during the test through its GSE, sampling each of its operating parameters once every four seconds. The LABVIEW files generated by this system were delivered to UofA from Creare. Each GSE telemetry record was time-correlated with the SITS science data files. For each science data readout, the 70 NCC telemetry items captured at the time closest to the end of the science data readout and were formatted and attached as keyword/value pairs in the science extension headers of the multiaccum FITS files. The NCC keywords were simply named NC0 - NC69, and carry brief descriptors identifying each value in the headers. Table 3.1 is an extract from a FITS header listing all NCC keyword entries with representative values. Of particular interest to this test are items NCS14 (compressor inverter frequency, Hz), NCS16 (compressor rotation speed, rps), NCS18 (turbo alternator speed, rps), and NCS19 (compressor motor current). Note that the compressor rotation speed will not be valid when the compressor motor is off. When the compressor motor is on NCS19 will have values ≥ 14 amps (higher at greater speeds), and close to zero when it is off.

```
┌─────────────────────────────────────────────────────────────────────────┐
│ Table  3.1.  NCC/GSE  Telemetry  Keywords/Values  in  FITS  Headers       │
│                                                                            │
│ NCS0    = 'old format'         / format                                    │
│ NCS1    =             26.915 / Bus Monitor (Volt x 7.97)                    │
│ NCS2    =              5.708 / 5.3 VDC Standby II (Volt)                    │
│ NCS3    =              0.012 / Comp. Spd. Lim O/R Ena.(Volt)                │
│ NCS4    =             -0.002 / Comp. Spd. Lim O/R Dis.(Volt)                │
│ NCS5    =              4.823 / Comp. On/off Cmd.(Volt)                      │
│ NCS6    =             -0.001 / Circ. On/off Cmd (Volt)                      │
│ NCS7    =              4.907 / Load Hi/lo Cmd (Volt)                        │
│ NCS8    =              4.869 / Freq.Limit O/R Status(Volt)                  │
│ NCS9    =              6.619 / Comp. Motor Current Cmd (Volt x 2.95)        │
│ NCS10   =             -0.001 / Circ. Invrt. Volt Cmd  (Volt x 1.5223 - 0.1223) │
│ NCS11   =              8.241 / Comp. Invtr. Freq. Cmd. (Volt x 796)         │
│ NCS12   =                -0. / Circ. Invrt. Freq. Cmd.(Volt x 200)          │
│ NCS13   =             15.165 / Analog Sel. Control (Volt)                   │
│ NCS14   =           6503.591 / Comp. Invt. Freq. (Volt x 711.7 -75.9)       │
│ NCS15   =             -0.124 / Circ. Invt. Freq. (Volt x 200)               │
│ NCS16   =           6367.016 / Comp. Rotat. Speed (Volt x 800)              │
│ NCS17   =              11.69 / Circ. Rotat. Speed (Volt x 201)              │
│ NCS18   =           3727.254 / Turbo Alt. Speed (Volt x 520.45 )            │
│ NCS19   =             19.522 / Comp. Motor. Current (Volt x 2.85 - 0.0456)  │
│ NCS20   =             -0.003 / Circ. Invrt. Current (Volt x 0.152  -0.009)  │
│ NCS21   =              0.617 / Circ. Invrt. Volt (Volt x 1.502)             │
│ NCS22   =              4.805 / TA Load Volt (Volt x 1.01)                   │
│ NCS23   =              7.788 / PCE Current (Volt x 6.0)                      │
│ NCS24   =             -0.004 / Freq. Limit Det. Status (Volt)               │
│ NCS25   =              0.008 / TA Load Hi/Lo Status (Volt)                  │
│ NCS26   =              0.005 / Comp. On/Off Status (Volt)                   │
│ NCS27   =              4.984 / Circ. On/Off Status (Volt)                   │
│ NCS28   =              308.5 / Load Interface T2(PRT) (TS04)                │
│ NCS29   =              303.4 / NICMOS Out T7(PRT)                           │
│ NCS30   =              301.3 / NICMOS In T3(PRT)                            │
│ NCS31   =              301.3 / T/A Housing T6(PRT)                          │
│ NCS32   =              305.5 / Circ Hsg T5(PRT) (TQ32)                      │
│ NCS33   =              29.02 / Comp. Base Plate (2.2K Therm)                │
│ NCS34   =              33.99 / Comp. Housing (2.2K Therm)                   │
│ NCS35   =               28.1 / Comp. Inlet (2.2K Therm)                     │
│ NCS36   =              24.16 / Neon Fill Bottle (2.2K Therm)                │
│ NCS37   =              24.44 / Neon Refill Bottle (2.2K Therm)              │
│ NCS38   =               25.1 / Neon Cap. Line (2.2K Therm                   │
│ NCS39   =              24.83 / Supply Valve (2.2K Therm)                    │
│ NCS40   =              26.72 / Heat Rejection (2.2K Therm)                  │
│ NCS41   =              27.98 / After Cooler (2.2K Therm)                    │
│ NCS42   =              23.96 / Solenoid Valve 1 (2.2K Therm)                │
│ NCS43   =              24.08 / Solenoid Valve 2 (2.2K Therm)                │
│ NCS44   =              23.93 / Manual Valve (2.2K Therm)                    │
│ NCS45   =             34.173 / Comp. Inlet Prs. (Volt. x 15.027 + 0.3306)   │
│ NCS46   =             50.649 / Comp. Out Prs. (Volt. x 20.085 + 0.4001)     │
│ NCS47   =              3.779 / Circ. Inlet Prs. (Volt. x 60.013 + 0.7451)   │
│ NCS48   =              0.043 / Circ. Diff. Prs. ((Volt. + * 1.998) +0.1142) │
│ NCS49   =              9.428 / Fill Bottle Prs. (Volt. x 59.992 + 0.5910)   │
│ NCS50   =              9.538 / Refill Bottle Prs. (Volt. x 59.945 + 0.5015) │
│ NCS51   =              32.25 / PCE Temperature  (2.2K Therm)                │
│ NCS52   =              5.495 / Power Status (Volt)                          │
│ NCS53   =                -0. / Survival Htr A Status (Volt)                 │
│ NCS54   =                -0. / Survival Htr B Status (Volt)                 │
│ NCS55   =             -0.161 / Total Comp. Current (Volt x 6)               │
│ NCS56   =              308.5 / Load Interface T2A(PRT) (TS29)               │
│ NCS57   =              301.9 / TA Inlet T8(PRT)                             │
│ NCS58   =              301.6 / NICMOS In T3A(PRT)                           │
│ NCS59   =              301.5 / T/A Inlet T8A(PRT)                           │
│ NCS60   =              303.7 / NICMOS Out T7A(PRT) (TS26)                   │
│ NCS61   =              0.019 / Power Supply (Volt)                          │
│ NCS62   =             26.731 / Bus volt. @ Sorenson                         │
│ NCS63   =             25.305 / Bus volt. @ EMI filter                       │
│ NCS64   =             11.029 / Bus Current Shunt (Volt x 1000)              │
│ NCS65   =              0.991 / TA Load Current (Volt x .200)                │
│ NCS66   =              8.111 / Comp. Invrt Input Current                    │
│ NCS67   =             167.25 / Comp. Invrt Out Power (Volt x 52.1 + 8.0)    │
│ NCS68   = 'Tue, Jun 27, 2000'  / Date                                       │
│ NCS69   = '4:04:05 PM'         / Time                                       │
└─────────────────────────────────────────────────────────────────────────┘
```

The "final" post-processed data files have been organized into directories corresponding to individual test segments (See section 4) and have been delivered to STScI on a set of four CD ROMS. Two CD ROMS contain data derived from test day 179, and two from test day 180. The data files on the "RAW" CD ROMS contain subdirectories named FITSxx{_x} which correspond to particular test segments which are described in Section 4. The "raw" files contained in these directories are the individual detector reads as simple FITS files before they were combined into the STScI multiaccum data format. The "root" file names contain the timetag of the transfer of the

science data through the SDF and uniquely identify the readout through a post-fixed incremental counter.

The data files on the EMI00179 and EMI00180 CDROMS may be of more immediate utility. The directories with the same names as on the RAW CD ROMs contain files which are in the STScI multiaccum format, and are identified by directory and root file name in the same manner. In each FITSxx{_x} subdirectory is a LOG file which identifies for each science extension how the image data was correlated with the NCC telemetry in the Labview data files (for example see a sample log file extract in Table 3.2).

The EMI00179 and EMI00180 CD ROMS also contain the NCC GSE telemetry in the LABVIEW subdirectories, in three formats. Files without any name extensions are in the original LABVIEW format delivered by Creare. Files of the same names with a .OUT extensions are tab delimited with records delimited by new-line characters so they are immediately amenable to be imported into spreadsheet programs such as Excel. Files with a .FITS extension are the same data written as FITS binary tables. Each of these files has headers of the appropriate format to identify the data fields (and corresponds to the FITS header keywords written onto the science data files).

Finally, we provide sets of "reference darks" made by median combining corresponding reads of multiple NCC OFF frames taken at a number of epochs during the test. These are the darks which were used in the analysis of the test data described elsewhere in this report. We provide them as a convenience for others who may wish to re-assess our results. These dark reference files may be found in subdirectories named DARKnn on the "RAW" CD ROMS. These dark reference files are also inverse time-ordered multiaccum .FITS files, so they may be immediately paired and subtracted from individual test data files of the same readout spacings and numbers. These "darks" were assembled from suites of individual frames identified in "dark.log" file accompanying the reference files on the CD ROM. The dark reference files carry the root name of the raw data plus "_DRK" of the chronologically first NCC OFF multiaccum which went into its construction. Also in these directories are files with corresponding names postfixed "_PIX", which gives for every pixel in each read, the number of individual readouts which went into making its reference value.

```
Table 3.2    Sample LOG file Correlating Image data and NCC Telemetry

06Jul2000 15:40:11 - NICMOS NCS Noise FITS + Labview Post Processing
Logfile:  fits2a-1.log

Processing I00179155504_2RUV4A1_PP.FITS with /labview/Jun27_02.out:obsdate=06/27/00 16:03:35UT
EXT   SAMPTIME        ISTEP  EXPTAG              TIMETAG             Labview Date+Time
 26   0.000    0      2000062716:03:35    2000062716:03:37    Tue, Jun 27, 2000 4:03:37 PM
 25   1.198    1      2000062716:03:36    2000062716:03:37    Tue, Jun 27, 2000 4:03:37 PM
 24   2.395    2      2000062716:03:37    2000062716:03:37    Tue, Jun 27, 2000 4:03:37 PM
                                                .
                                                .
                                                .
 3    27.543   28     2000062716:04:03    2000062716:04:05    Tue, Jun 27, 2000 4:04:05 PM
 2    28.740   29     2000062716:04:04    2000062716:04:05    Tue, Jun 27, 2000 4:04:05 PM
 1    29.938   30     2000062716:04:05    2000062716:04:05    Tue, Jun 27, 2000 4:04:05 PM
26 extensions updated (see I00179155504_2RUV4A1_PP.FITS)
                                                .
                                                .
                                                .
```

4. TEST SEGMENTS (A Summary/Guide to The EMI Test Data Collection)

Testing was carried out over three days using a combination of stored command load segments generated from two science Mission Specifications, and real-time commanding. Both stored and real-time command segments were executed on a SITS system communicating with the GSFC VEST/NICMOS-BRZ replica flight electronics. Early on the first test day, day 178, the SITS system failed. While some preliminary data was obtained with the NCC OFF (and used to validate the test set up), these were not used in the EMI and system noise analyses and are not discussed further. The problem was subsequently resolved and testing resumed on day 179. All data discussed in this report, and delivered to STScI, were obtained on days 179 and 180.

The EMI data frames collected and used in our analyses consisted of repeated series of differential measures obtained with the NCC OFF, and with the compressor running at a variety of speeds. Three different methods of sampling were employed, with primary emphasis given to collecting sets of three 26-read multiaccums with 1.2 seconds between readouts. This sampling strategy was employed in the April, 1998 EMI test where the original ~ 6-9 kHz broadband EMI problem was identified,. We defer to that test report to further describe the rational for this sampling strategy. In addition, at the request and specification of STScI additional data collections were made using asynchronous delta times between reads, and using STEP64 sampling, exactly replicating one of the commonly used detector integration timing sequences used on orbit. Finally, sets of 30 back-to-back 2-read multiaccum frames, used to evaluate the read-noise, were taken by a real-time procedure, and hence are not on either of the SMSs. These frames were taken at the start and end of each day, whenever we changed a mechanical or electrical configuration, or occasionally to measure the stability of the read-noise.

These four data collection sequences are identified in the test segment summary as follows:

```
  RN "Read Noise"       30   2-read 1.2s integration MA frames
  UA "UofA Sequence"     3  26-read 1.2s delta time MA frames
  ST "STScI Sequence"    5  10-read asynchronous delta time MA frames
  S2 "SMS2 Long Seq"     4  STEP64 MA frames - Long integrations (SMS2)
```

The UA sequences (which are the focus of the analysis in this report) were interleaved on SMS1 with the ST sequences. In Table 4.1 the test-segment image sequences are presented in chronological order, along with very brief explanatory notes of the H/W configuration. The timetags, such as 178151503, give the time that the data were "dumped" from the NICMOS replica electronics, and are attached as part of the file names for that execution of the particular sequence. The same timetag name appears for all sequential repeats (e.g., 3 of UA, or 5 of ST). Unique file name identifiers, which increase monotonically, are postpended to the timetags. The UA, ST, and S2 sequences were reformatted as multiple science extension multiaccum FITS files on the DAY0179 and DAY180 CD ROMS. The RN sequences are provided only as simple single-read FITS files, so the set of 30 RN exposures are constituted by a set of 60 files of (first, last) read pairs, named sequentially (monotonically) in their directories.

The execution order of these sequences is somewhat in variance with the pre-approved test plan (Hubble Space Telescope FS&S Project, NCC/NICMOS EMI Noise Test, I&T Ptocedure, P-442-2488). This was done to accommodate problems we had due to SITS failures, preemptive shut downs due to local lightning storms (storm code confition 3), and authorization to run the cooler at speeds in excess of 6500 rps for protracted (< 20 minute) durations.

```
                    Table 4.1    Test and Data Segment Summary


Shorted Buffer Box Test (BRZ Check Out)
.................................................................
178/0a    178151503 RN  30 SBB              NCC GSE OFF  Not Grounded

Detector Operations Test
.................................................................
178/0b    178175742 RN  30 Detector        NCC GSE ON   Not Grounded

.................................................................
ESTABLISH HST-LIKE GROUND CONNECTIONS NCC/DETECTOR

Initial Read Noise Evaluation for Test Configuration
.................................................................
178/0c    178185936 RN  30 Detector        NCC GSE ON

Initial Dark Frames to make "super dark" medians
.................................................................
178/0d-1 178191704 UA   3 Detector         NCC GSE ON
178/0d-2 178192209 ST   5 Detector         NCC GSE ON
178/0d-1 178192526 UA   3 Detector         NCC GSE ON
178/0d-2 178193031 ST   5 Detector         NCC GSE ON
178/0d-1 178193348 UA   3 Detector         NCC GSE ON


.................................................................
POD File CSIN00178193348 corrupted, 178193853 and 178194210 bad
SITS System Failure - No Data for Remainder of Day

.................................................................
BRZ OFF, DEWAR REMOVAL, PUMP OVERNIGHT, AM REFILL

Day 179 Initial Read Noise Frames
.................................................................
179/0a    179124242 RN  30 Detector        NCC OFF

Day 179 Dark Frames to make "super dark" medians
.................................................................
179/0b-1 179130004 UA   3 Detector         NCC OFF
179/0b-2 179130509 ST   5 Detector         NCC OFF
179/0b-1 179130826 UA   3 Detector         NCC OFF
179/0b-2 179131331 ST   5 Detector         NCC OFF
179/0b-1 179131648 UA   3 Detector         NCC OFF
179/0b-2 179133253 ST   5 Detector         NCC OFF
179/0b-1 179132510 UA   3 Detector         NCC OFF
179/0b-2 179133015 ST   5 Detector         NCC OFF


.................................................................
Ground Strap Conductance Measurements Made
Lights in EMI Clean Room Turned Off (flickering flourscent)

Darks to Verify No Change after Conductance Measures
.................................................................
179/0c-1 179141204 UA   3 Detector         NCC OFF
179/0c-2 179141709 ST   5 Detector         NCC OFF
179/0c-1 179142026 UA   3 Detector         NCC OFF
179/0c-2 179142531 ST   5 Detector         NCC OFF


.................................................................
CLI Heater Turned Off to Check for Additional Noise Signatures

Darks to Verify CLI Heater Lines Are Not a Noise Source
.................................................................
179/0c-1 179142848 UA   3 Detector         NCC OFF
179/0c-2 179143353 ST   5 Detector         NCC OFF
```

```
179/0c-1 179143710 UA   3 Detector        NCC OFF
179/0c-2 179144215 ST   5 Detector        NCC OFF


..........................................................................
CLI Heater Turned Back On

NCS Operations @ 5500 rps
..........................................................................
179/1a-1 179151304 UA   3 Detector        NCC ON   5500 rps
179/1a-2 179151809 ST   5 Detector        NCC ON   5500 rps
179/1a-1 179152126 UA   3 Detector        NCC ON   5500 rps
179/1a-2 179152631 ST   5 Detector        NCC ON   5500 rps
179/1a-1 179152948 UA   3 Detector        NCC ON   5500 rps
179/1a-2 179153453 ST   5 Detector        NCC ON   5500 rps
179/1a-1 179153810 UA   3 Detector        NCC ON   5500 rps
179/1a-2 179154315 ST   5 Detector        NCC ON   5500 rps

NCS Operations @ 6500 rps

..........................................................................
179/2a-1 179155004 UA   3 Detector        NCC OFF
179/2a-2 179160009 ST   5 Detector        NCC OFF
179/2a-1 179160326 UA   3 Detector        NCC RAMP UP
179/2a-2 179160831 ST   5 Detector        NCC RAMP UP
179/2a-1 179161148 UA   3 Detector        NCC ON   6500 rps
179/2a-2 179161653 ST   5 Detector        NCC ON   6500 rps
179/2a-1 179162010 UA   3 Detector        NCC ON   6500 rps
179/2a-2 179162515 ST   5 Detector        NCC ON   6500 rps

NCS Operations @ 7200 rps (max 20 minute on time)

..........................................................................
179/3a-1 179165504 UA   3 Detector        NCC OFF
179/3a-2 179170009 ST   5 Detector        NCC RAMP 5500-6750 rps
179/3a-1 179170326 UA   3 Detector        NCC RAMP 6750-7200 rps
179/3a-2 179170831 ST   5 Detector        NCC ON    7200 rps
179/3a-1 179171148 UA   3 Detector        NCC ON    7200 rps
179/3a-2 179171553 ST   5 Detector        NCC ON    7200 rps
179/3a-1 179170210 UA   3 Detector        NCC ON    7200 rps
179/3a-2 179172515 ST   5 Detector        NCC ON    7200 rps


..........................................................................
NCC OFF for cool down

Read Noise Evaluation
..........................................................................
179/0d    179174337 RN 30  Detector        NCC OFF

NCS Operations @ 7000 rps (20 minute maximum)
..........................................................................
179/4a-1 179175304 UA   3 Detector        NCC OFF
179/4a-2 179175809 ST   5 Detector        NCC OFF
179/4a-1 179180126 UA   3 Detector        NCC RAMP 5500-7000 rps
179/4a-2 179180631 ST   5 Detector        NCC ON    7000 rps
179/4a-1 179180948 UA   3 Detector        NCC ON    7000 rps
179/4a-2 179181453 ST   5 Detector        NCC ON    7000 rps
179/4a-1 179181810 UA   3 Detector        NCC ON    7000 rps
179/4a-2 179182315 ST   5 Detector        NCC ON    7000 rps


..........................................................................
NCC OFF for cool down

NCS Operations @ 6800 rps (20 minute maximum)
..........................................................................
179/5a-1 179185404 UA   3 Detector        NCC OFF
179/5a-2 179185909 ST   5 Detector        NCC OFF
179/5a-1 179190226 UA   3 Detector        NCC RAMP to 6800 rps
```

```
179/5a-2 179190731 ST    5 Detector        NCC ON    6800 rps
179/5a-1 179191048 UA    3 Detector        NCC ON    6800 rps
179/5a-2 179191553 ST    5 Detector        NCC ON    6800 rps
179/5a-1 179191911 UA    3 Detector        NCC ON    6800 rps
179/5a-2 179192415 ST    5 Detector        NCC ON    6800 rps

.................................................................
NCC OFF for cool down

NCC Operations @ 6200 rps
.................................................................
179/6a-1 179194305 UA    3 Detector        NCC OFF
179/6a-2 179194809 ST    5 Detector        NCC OFF
179/6a-1 179195129 UA    3 Detector        NCC RAMP to 6200 rps
179/6a-2 179195631 ST    5 Detector        NCC ON    6200 rps
179/6a-1 179195948 UA    3 Detector        NCC ON    6200 rps
179/6a-2 179200453 ST    5 Detector        NCC ON    6200 rps
179/6a-1 179200810 UA    3 Detector        NCC ON    6200 rps
179/6a-2 179201315 ST    5 Detector        NCC ON    6200 rps

.................................................................
NCC OFF for cool down

Dark Frames for SMS-2 (STEP64 Integrations)
.................................................................
179/7a   179210356 S2    4 Detector        NCC OFF (SMS2)

.................................................................
NCC RAMP up to 6500 rps before SMS Start

NCS Operations @ 6500 rps
.................................................................
179/7b   179215056 S2    4 Detector        NCC ON 6500 rps (SMS2)

.................................................................
NCS OFF (end of day, weather code 3, lightning storms in area)

Day 179 Final Read Noise Evaluation
.................................................................
179/0e   179220955 RN   30 Detector        NCC OFF

.................................................................
BRZ OFF, DEWAR REMOVAL, PUMP OVERNIGHT, AM REFILL
DEWAR RE-INTEGRATED, GROUND STRAPS ATTACHED, CURRENT PROBE REMOVED

Day 180 Initial Read Noise Evaluation
.................................................................
180/0a   180124047 RN   30 Detector        NCC OFF

NCC Operations @ 7200 rps (repeatability from day 179, 20 minute max)
.................................................................
180/1a-1 180124904 UA    3 Detector        NCC OFF
180/1a-2 180125498 ST    5 Detector        NCC OFF
180/1a-1 180125726 UA    3 Detector        NCC RAMP 7000-7200 rps
180/1a-2 180130231 ST    5 Detector        NCC ON    7200 rps
180/1a-1 180130548 UA    3 Detector        NCC ON    7200 rps
180/1a-2 180130553 ST    5 Detector        NCC ON    7200 rps
180/1a-1 180131410 UA    3 Detector        NCC ON    7200 rps
180/1a-2 180131915 ST    5 Detector        NCC ON    7200 rps

.................................................................
NCC OFF for cool down

NCC Operations @ 6100 rps
.................................................................
180/2a-1 180134204 UA    3 Detector        NCC OFF
```

```
180/2a-2 180134709 ST   5 Detector          NCC OFF
180/2a-1 180135531 UA   3 Detector          NCC RAMP to 6100 rps
180/2a-2 180130231 ST   5 Detector          NCC ON   6100 rps
180/2a-1 180135848 UA   3 Detector          NCC ON   6100 rps
180/2a-2 180140353 ST   5 Detector          NCC ON   6100 rps
180/2a-1 180140710 UA   3 Detector          NCC ON   6100 rps
180/2a-2 180141215 ST   5 Detector          NCC ON   6100 rps

NCC Operations @ 6200 rps
...............................................................
180/3a-1 180142104 UA   3 Detector          NCC OFF
180/3a-2 180142609 ST   5 Detector          NCC OFF
180/3a-1 180142926 UA   3 Detector          NCC RAMP to 5900 rps
180/3a-2 180143431 ST   5 Detector          NCC ON   5900 rps
180/3a-1 180143748 UA   3 Detector          NCC ON   5900 rps
180/3a-2 180144253 ST   5 Detector          NCC ON   5900 rps
180/3a-1 180144610 UA   3 Detector          NCC ON   5900 rps
180/3a-2 180145115 ST   5 Detector          NCC ON   5900 rps

Read Noise Evaluation
...............................................................
180/0b   180151040 RN  30 Detector          NCC OFF

NCC Operations @ 5700 rps
...............................................................
180/4a-1 180151804 UA   3 Detector          NCC OFF
180/4a-2 180152309 ST   5 Detector          NCC OFF
180/4a-1 180152626 UA   3 Detector          NCC RAMP to 5700 rps
180/4a-2 180153131 ST   5 Detector          NCC ON   5700 rps
180/4a-1 180153448 UA   3 Detector          NCC ON   5700 rps
180/4a-2 180153953 ST   5 Detector          NCC ON   5700 rps
180/4a-1 180154310 UA   3 Detector          NCC ON   5700 rps
180/4a-2 180154815 ST   5 Detector          NCC ON   5700 rps

NCC Operations @ 5000 rps
...............................................................
180/5a-1 180155804 UA   3 Detector          NCC OFF
180/5a-2 180160309 ST   5 Detector          NCC OFF
180/5a-1 180160626 UA   3 Detector          NCC RAMP to 5000 rps
180/5a-2 180161131 ST   5 Detector          NCC ON   5000 rps
180/5a-1 180161448 UA   3 Detector          NCC ON   5000 rps
180/5a-2 180161953 ST   5 Detector          NCC ON   5000 rps
180/5a-1 180162310 UA   3 Detector          NCC ON   5000 rps
180/5a-2 180162815 ST   5 Detector          NCC ON   5000 rps

Read Noise Evaluation
...............................................................
180/0c   180180728 RN  30 Detector          NCC OFF

...............................................................
COOLER MOVED CLOSER TO DEWAR.  DISTANCE CLOSURE FROM 3FT. TO 1FT.
WORST-CASE RADIATED EMISSIONS SUSCEPTIBILITY

Read Noise Evaluation
...............................................................
180/0d   180183710 RN  30 Detector          NCC OFF

NCC Operations @ 7200 rps (repeatability @ 1ft distance)
...............................................................
180/6a-1 180184604 UA   3 Detector          NCC OFF
180/6a-2 180185109 ST   5 Detector          NCC OFF
180/6a-1 180185426 UA   3 Detector          NCC RAMP 7000-7200 rps
180/6a-2 180185932 ST   5 Detector          NCC ON   7200 rps
180/6a-1 180190248 UA   3 Detector          NCC ON   7200 rps
```

```
180/6a-2 180190753 ST   5 Detector        NCC ON   7200 rps
180/6a-1 180191110 UA   3 Detector        NCC ON   7200 rps
180/6a-2 180191615 ST   5 Detector        NCC ON   7200 rps

..................................................................
NCC OFF for cool down

NCC Operations @ 7200 rps SMS2
..................................................................
180/7a   180201456 S2   4 Detector        NCC ON 7200 rps (SMS2)

Dark Frames for SMS2
..................................................................
180/7b   180210156 S2   4 Detector        NCC OFF (SMS2)

Dark Frames for SMS1
..................................................................
180/0e-1 180211304 UA   3 Detector        NCC OFF
180/0e-2 180211809 ST   5 Detector        NCC OFF
180/0e-1 180212126 UA   3 Detector        NCC OFF
180/0e-2 180212631 ST   5 Detector        NCC OFF
180/0e-1 180212949 UA   3 Detector        NCC OFF
180/0e-2 180213453 ST   5 Detector        NCC OFF
180/0e-1 180213810 UA   3 Detector        NCC OFF
180/0e-2 180214315 ST   5 Detector        NCC OFF

Read Noise Evaluation
..................................................................
180/0f   180220100 RN  30 Detector        NCC OFF

..................................................................
BRZ OFF, DEWAR REMOVAL, BEGIN WARM-UP
```

5. DETECTOR CHARACTERISTICS, THERMAL STABILITY & DEWAR MAINTENANCE

The NICMOS flight spare detector #97T0012 and the test dewar employed have significant pedigrees and both are well characterized and calibrated. This detector/dewar combination was used in the 1998 EMI test, and again in fall of 1999 over a period of many weeks to replicate the on-orbit warm-up of NICMOS and investigate some unexpected behaviors seen during the period of thermal transition in the flight detectors after cryogen exhaustion. The detector, and dewar with its optical entrance port blanked off, were integrated and configured identically to that test, and we defer to that post-test report, NICMOS ISR-00-002, available at the STScI web site to describe the characteristics of the hardware also employed for the EMI test.

For the EMI test, the NICMOS-3 detector was cooled by liquid Nitrogen (LN2). With LN2, the hold-time between dewar refills (at sea level) is ~ 12 hours. Because of the added complexity which would have been required to perform dewar pumping, refill, and maintenance operations in the EMI clean-room environment, the dewar was removed for servicing between test days. Prior to (re)integration in the clean-room, the dewar was pumped to establish a hard vacuum, and refilled with LN2. The detector was allowed to stabilize for a minimum of 3 hours after equilibrating at 77.30K before any image data were taken. For all test data obtained, the detector was maintained at a temperature of 77.30 +/-0.01K (see Figure 1.1).
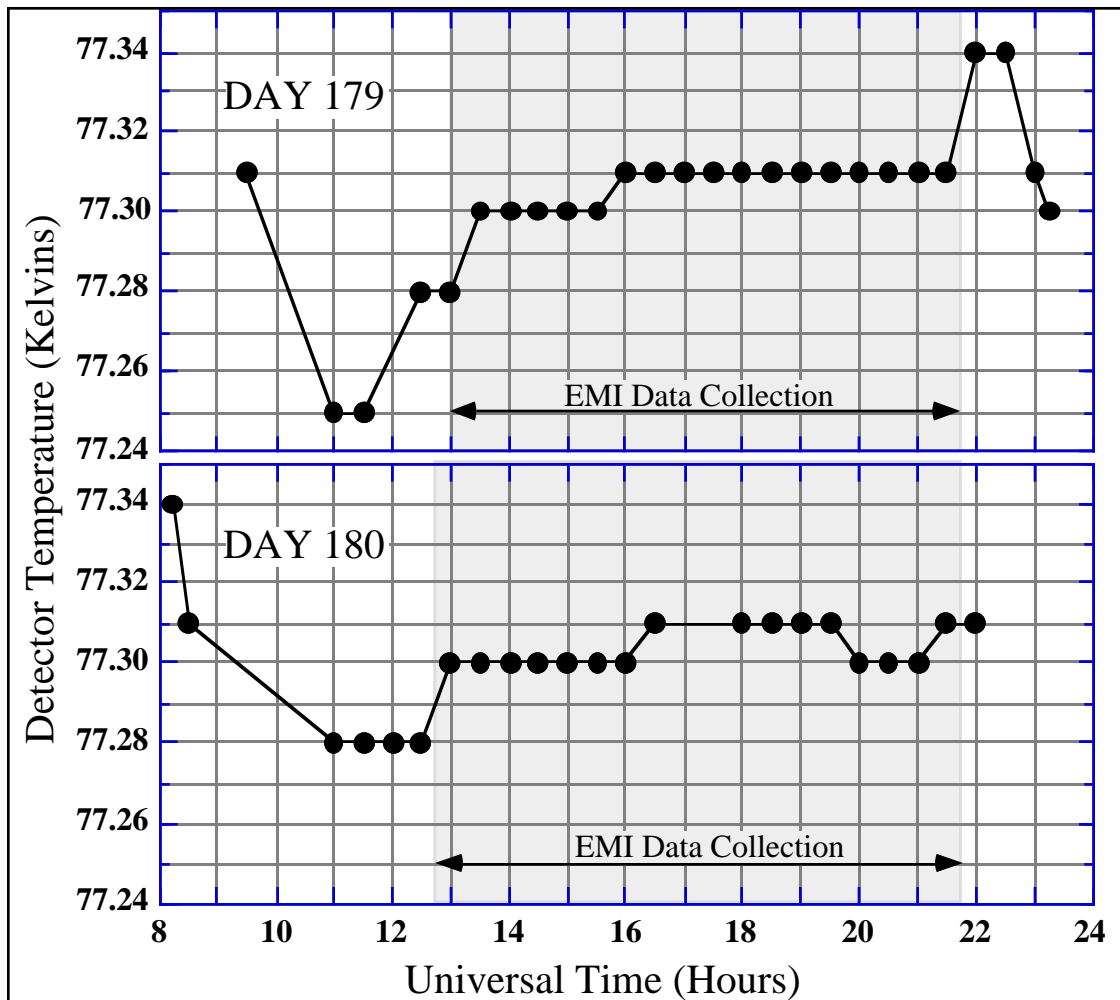
Figure 5.1. During EMI data collection (NICMOS-3 imaging) on both days 179 and 180 (from ~ 13 to 22 hours U.T.,) the flight spare detector was maintained at a cryogenic temperature of 77.30 +/-0.01K.

6. READ NOISE ASSESSMENT

The detection and measurement of external signals impressed in the read-outs of each photodiode in the NICMOS-3 flight-spare focal plane array depends upon the intrinsic noise characteristics of the detector and of the NICMOS replica electronics. The ability to differentiate between local environmental signal contamination (i.e., incomplete shielding of non-NCC related interference in the screen room) rests in performing well characterized differential source and background measures. The "read-noise" of the system was periodically measured to evaluate the systemic sensitivity to both intrinsic and extrinsic noise sources. Here, we carefully define "read-noise" to mean the non-repeatability in the measurement of the signal accumulation from data collected by a single photodiode on the NICMOS-3 detector plus the contribution to that measurement uncertainty from the downstream readout electronics.

The measurement of the accumulating signal applied to all pixels, which can have negative measures due to a time-decaying device reset signal known as "shading", may be summarized as follows. First, all pixels are sequentially reset. Second, after turning on the on-chip amplifiers and waiting 28ms for stabilization, the signals on all photodiodes are sequentially measured to establish a reference (DC bias) level for each pixel. Third, after shutting down the amplifiers, and waiting 1.2s, each pixel is sequentially re-read in the same manner. In these three steps a 10.49 microsecond horizontal pixel clock is used to access pixels, and each 128-pixel row (simultaneously clocked in each of the four detector quadrants) is overclocked by two cycles of the horizontal clock. This is identical to what is done in flight. The initial read is then subtracted from the final read to obtain a single read-pair difference-image of all pixels on the device. This process is repeated thirty times to obtain a set of read-noise limited images. We refer to this repeated imaging sequence as the RN series.

Measurement values in individual reads are quantized due to the finite precision of the NICMOS replica's 16-bit analog-to-digital converters . Hence, difference images in the read-pair measures, are also quantized. We combine the thirty difference frames into a final image (for example, see Figure 6.1) doing a 3-sigma clipping about the median, throwing out outliers (of which there usually are none), and then computing a post-clipped mean. For a sample size of 30 this obviates the discrete quantization limitation in assessing the per-pixel noise characteristics. A sample final image from a RN series combined in this manner is shown in Figure 6.1, with vertical profiles of the major artifacts discussed in Figure 6.2.

Figure 6.1. A post-medianed 3-sigma clipped mean image, from a set of thirty 1.2s integration 2-read multiaccum difference-images (RN series), shows the characteristic image artifacts for this detector. The brightening in the four corners is due to amplifier glow. The broad light and dark bands at the bottom of each quadrant (accessed first in time order; time increasing to the right and up) is the signature of 20-row re-clocking over the shading decay after resetting all pixels. The bright spots are hot pixels. In addition, a faint nearly horizontal band, a few pixels wide is seen ~ 1/3 the way "up" from the bottom of each quad in this image (~ rows 55 and 183; also see Figure 6.2). This is seen as a very sharp, noisy feature, but low S/N in individual (uncombined) difference frames, which very slowly drifts with time (and hence location on the detector) and varied in amplitude. This signal is apparently of short duration (about a millisecond), and almost, but not quite phase locked with the readouts. It undoubtedly arises in the BRZ replica electronics. This artifact has no significant effect on these test data, but we mention it as it appears in a large fraction of the data frames obtained in this test.
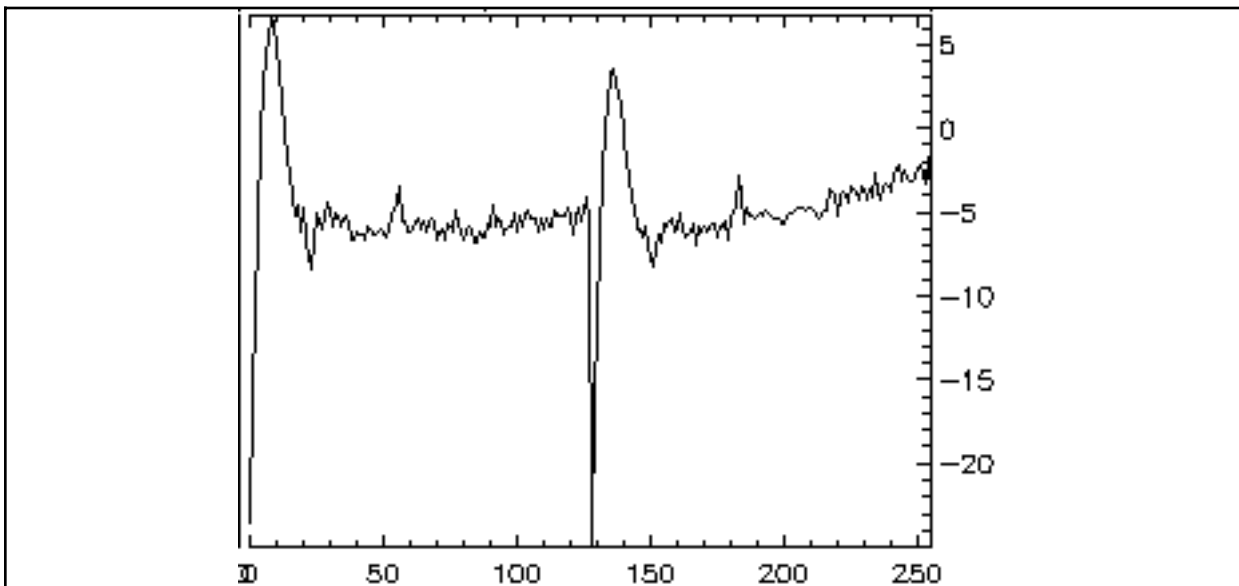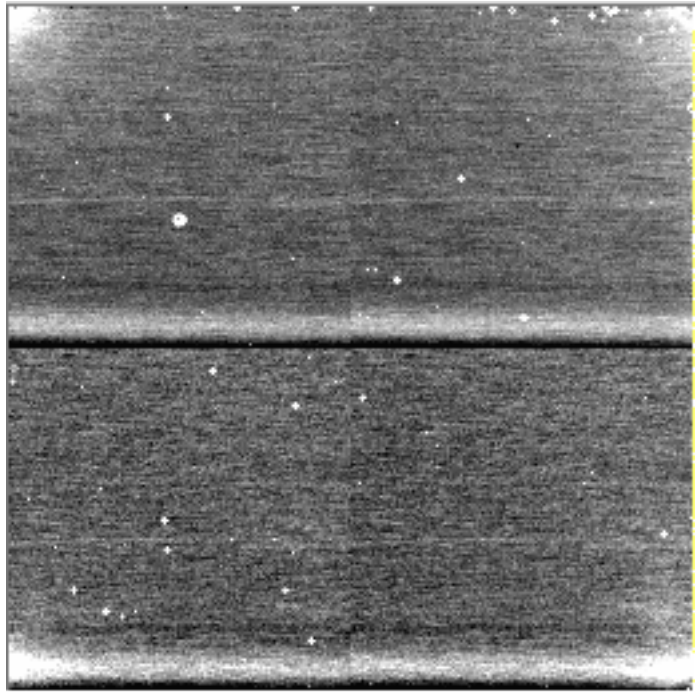
Figure 6.2. A row-collapsed median across both pairs of quads to illustrates the global structural characteristics in the RN images. Time collapsed along each row increases to the right (upward in the corresponding image, Figure 6.1). The reclocked shading signature is apparent. The higher amplitudes at the left and right edges are due to the superposition of the corner amplifier glows. The median value of the accumulated signal in the regions away from these strongly effected areas is ~ - 5 DN. This negative signal is purely due to the recovery of the shading decay for a 1.2s integration following the reset of this device.

For each pixel in the array, the 1-sigma deviations in measurement repeatability (with respect to the 3-sigma clipped mean image) defines the systemic read-noise per single read-pair per pixel. Figure 6.3 shows a representative standard deviation (1-sigma read-noise) image derived from a RN series.

Figure 6.3. Typical read-noise assessment image made from a set of 30 difference frames. The image, which provides a global read-noise map of each pixel, is displayed with a stretch from 4 to 19 DN (~ 22 to 103 electrons). Quadrants 1 and 2 (bottom, left and right, respectively) are noisier (hence brighter in this standard-deviation image) than quadrants 3 and 4 (top, right and left, respectively) due to differences in the intrinsic properties of the pre-amplifiers on the DES circuit boards.
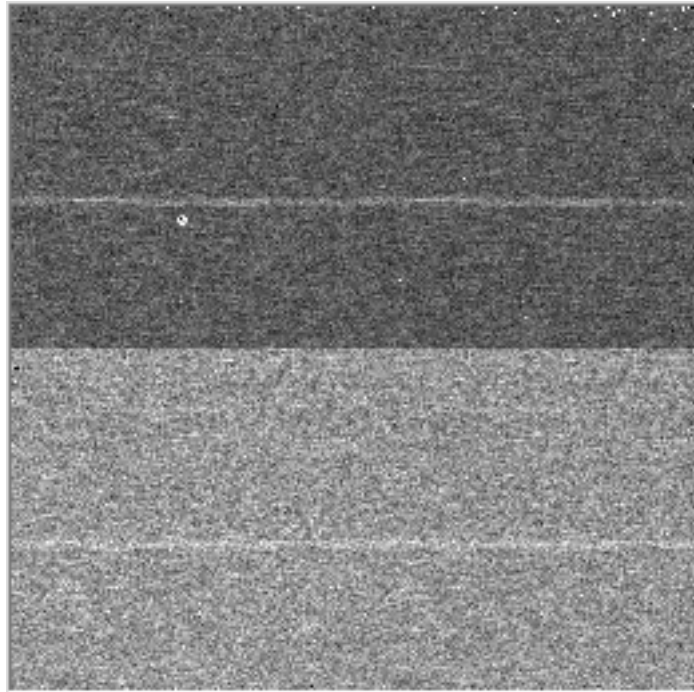
Two features in the read-noise image are noticed. First, quads 3 and 4 (top right and left, respectively) are noisier with mean per pixel read-noise values of ~ 13.4 DN, compared to quads 1 and 2 with mean per pixel read-noise values of ~ 9.7 DN. This is a consequence of the use of different preamps for these paired quads on different readout electronics circuit boards. This causes a broadening and bi-modal nature of the histogram of read-noise values over all pixels (Figure 6.4).
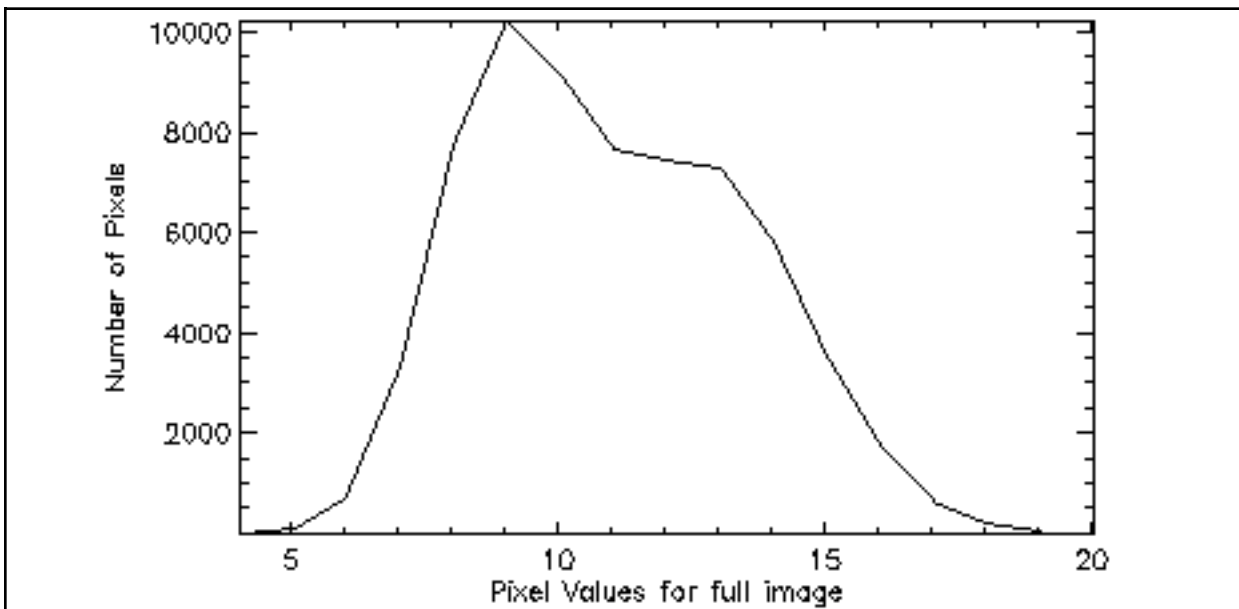
Figure 6.4. The distribution function of read-noise values (in DN, horizontal axis) over all pixels in the array is actually the linear superposition of two Gaussian distributions. The read-noise in pixels in quads 3 and 4 have characteristic values ~ 14% higher than those in quads 1 and 3.

The faint horizontal bands described in connection with the signal image in Figure 6.2 are readily apparent as "noise bands" in the corresponding read-noise image in Figure 6.4. In a row-median plot of the read-noise image, collapsed along the direction of the fast (horizontal) pixel clock (Figure 6.5), the "noise band" centered on row 55, and simultaneously repeated in quads 3 and 4 at row 183, is evident in the read-noise image. The read-noise is locally increased by ~15% in the affected pixels. This quasi-synchronous signal did drift with time, however, it resulted in no significant degradation in the visibility of EMI induced signals in the image frames.
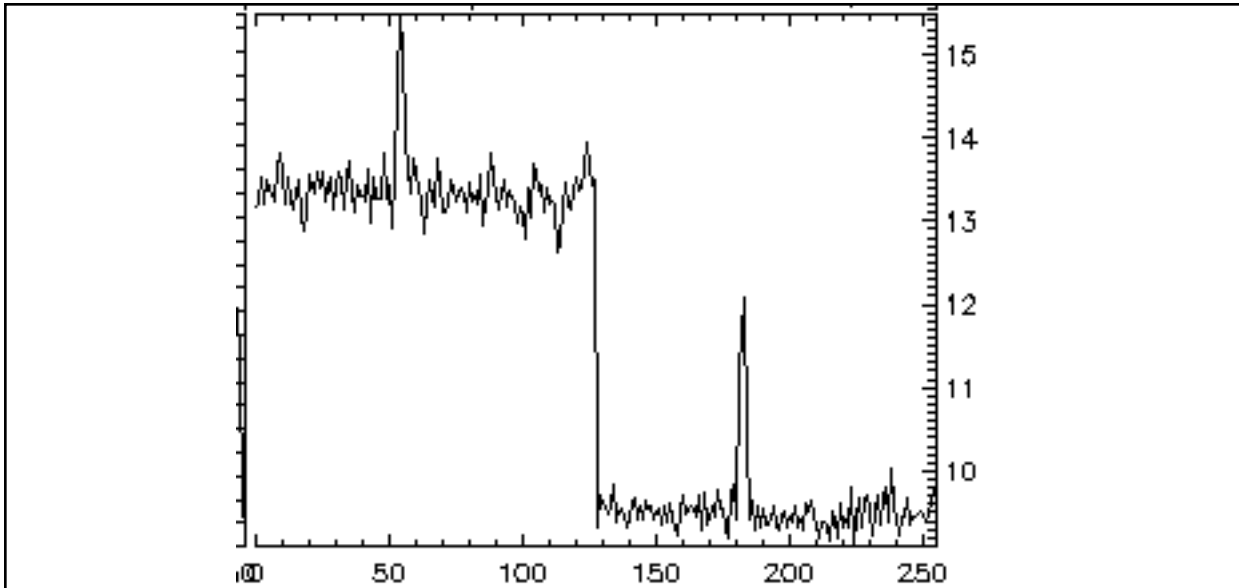
Figure 6.5 . A row-collapsed median plot made from the read-noise image in Figure 6.3. Time increases to the right, 1363.7 microseconds per row simultaneously in quads 1&4 (columns 0-127) and 2&3 (columns 128-255). Row numbers on the X-axis of this plot correspond to the vertical direction, from the bottom up, in Figure 6.3.

To assess the amplitude and monitor the stability of the system read-noise temporally contiguous RN series evaluation frames were obtained on eight occasions during the two days of NCC/EMI data collection. The RN sequences were executed by real-time command at key junctures during testing, and hence not appear in the stored command loads which were used to acquire the NCC/EMI data. Table 6.1 identifies by data set ID, and time, when the RN data were taken during the two days of testing.

```
         TABLE  6.1  -  Chronology  of  Read  Noise  Evaluations

179/0a 179124242 Initial Assessment Before First Dark Frames
179/0d 179174337 Following NCC 7200 rps (maximum) Run
179/0e 179220955 End of Day 179 Assessment

180/0a 180124047 Start of Day Assessment After Dewar Reintegration
180/0b 180151040 Following NCC 6200 rps Run
180/0c 180180728 Just Prior to Moving Dewar/NCC to 1ft Proximity
180/0d 180183710 Just After Moving Dewar/NCC to 1ft Proximity
180/0f 180220100 End of Day 180 Assessment
```

The *characteristic* read-noise for all pixels in a quadrant may be expressed by the standard deviation in the assemblage of individual pixel read-noise measures about a characteristic value (e.g., the median or sigma-clipped mean). Given the large number of pixels in a quadrant, the median and clipped mean values give very similar results. In this report we adopt the later as our comparative metric. Table 6.2 summarizes the read-noise statistics from the set of 30 RN images illustrated in Figures 6.1-6.5. We present the statistics computed over the distribution of all 64K pixels in the array only as a reference. It must be emphasized that impressed signals due to EMI

were measured *independently* in each of the four quadrants, so quads 3 and 4 provide slightly better sensitivity (reduced noise) than quads 1 and 2. In Appendix B we provide these statistics for all eight epochs of read-noise measures to illustrate stability, amplitude, and nature of the read-noise and standard deviation frames obtained throughout the test.

```
        TABLE 6.2 - Read-Noise (in DN) Statistics for 179/0a

              ALL Quads   Quad #1     Quad #2      Quad #3      Quad #4
Mean             11.563     13.593      13.302        9.667        9.679
Variance         52.575     22.535       3.338      167.642       85.094
Std Deviation     7.251      4.747       1.827       12.948        9.225
Clipped Mean     11.488     13.515      13.291        9.462        9.570
Clipped SDV       2.524      1.855       1.782        1.466        1.425
Bad Pixels          25          8          46            9           14
Total           757797     222704      217933       158378       317156
Median           11.22      13.48       13.27         9.41         9.52
Minimum           0.00       0.00        6.39         0.00         0.00
Maximum        1159.40     393.76       40.36      1159.40      1159.40
```

Thus far, we have expressed noise amplitudes in Data Numbers (counts output from the A-to-D converters). In this instrumental system a change of one data number (DN) equates a change in input signal of 5.4 electrons. This is essentially identical to NICMOS Cameras 1 and 2. In flight, the characteristic read-noise per 2-read pair measured in this manner is about 35 electrons for all four quadrants of all three cameras. In Table 6.3 we give the characteristic read-noises measured in each of the quads of the test detector for the epochs of testing described in Table 6.1, which were found to be very stable throughout testing.

```
     TABLE 6.3 - Read-Noise per 2-read difference (electrons)

   Dataset Timetag      -------------Quadrant------------
   DOY/##  DDDHHMMSS     1      2      3      4    Combined
   179/0a  179124242   73.0   71.8   51.1   51.7      31.0
   179/0d  179174337   67.7   66.8   52.2   52.7      30.0
   179/0e  179220955   67.0   66.0   51.6   52.1      29.6
   180/0a  180124047   76.6   75.3   54.4   55.0      32.7
   180/0b  180151040   70.2   69.2   53.8   54.2      31.0
   180/0c  180180728   69.8   68.8   53.6   54.1      30.9
   180/0d  180183710   69.5   68.6   53.4   53.9      30.7
   180/0f  180220100   69.1   68.1   53.1   53.5      30.5

   Mean over all        70.4   69.3   52.9   53.4      30.8
```

The "quietest" quads, 3 and 4, are about 50% noisier than in flight. However, impressed signals with frequencies below the ~ 50 Khz Nyquist cut-off of the NICMOS sampling are nearly simultaneously sampled in each of the four quads (within 250 nanoseconds of a 10.49 microsecond clock). Thus, an EMI induced signal is measured in all 4 quads and produces a correlated result. In our EMI data analysis, discussed later, we take advantage of having four such independent measures by averaging power spectra derived from each quadrant separately. By using four simultaneously accessed pixels (one in each quad) to sample the spatial frequencies of impressed signals, the read-noise is effectively reduced by root(4) weighted by the read-noise in each pixel. The last column in Table 6.3 gives the *effective* read-noise form the 4-pixel sets of correlated measures used in the EMI signal analysis. Thus, combined and averaged over the two days of testing, we find the characteristic effective read-noise in four simultaneously read pixels of 30.8 electrons, with a 1-sigma dispersion in the read-noise of ~ 9 electrons, and stability of the peak of the noise distribution to +/- 1 electron. This is very similar to the performance and sensitivity levels seen in flight when measuring the flux on a pixel in a similar manner. Hence, the fidelity of this test with respect to on-orbit read-noise limitations, is very high.

7. ABSOLUTE CALIBRATION

The periodic read-noise measures confirmed that the test system had a comparable read-noise floor to NICMOS on-orbit. Hence both systems should have roughly equal measurement sensitivities (though not necessarily susceptibility) to EMI induced signals. To quantitatively ascertain the signal detection limits in the presence of on-orbit like read-noise, we numerically injected control signals of known frequencies and amplitudes into individual reads of NCC OFF multiaccum exposures. This was done by these coadding adding fixed sinusoidal pattern noise (overclocked by two pixels) into each quadrant of observed MA reads. After subtracting an appropriate "super" dark reference file, power spectral analyses of these hybrid frames recovered the tracer signals, thereby allowing unambiguous calibration of the EMI noise component amplitudes. All of the test data were contaminated with 60Hz and third-harmonic 180Hz noise undoubtedly coupled at a low level from facility power. These non-NCC signals were prevalent whether the cooler was operating or not, so differentially, they are not a concern. These 60/180 Hz signals can also serindipitously serve as tracers. Their noise amplitudes, which varied on long time-scales compared to the read-out rate, were directly measured in the spatial domain (and found to be a few tens of DNs peak-to-peak). From this, their contributions to exceedences in 1/f noise spectra were determined.

As an example, consider Figure 7.1. The top left panel is a synthetic noiseless (i.e., no read-noise) NICMOS image with a 20 DN (+/-10 DN peak-to-peak) 6530 Hz sinusoidal signal impressed. In this case the horizontal spacing of the signal peaks every 14.599 pixels (spatial frequency = 0.06845 pixel^{-1} given the 10.49 microsecond pixel clock). When the pattern noise "wraps" in each quadrant there is a phase delay of two clock cycles (20.98 microseconds) to allow for the two pixel overclocking associated with the overhead for the vertical line clock management. Such synthetic signals, but of varying amplitudes and frequencies, were created to be coadded into different NCC OFF multiaccum reads. Here, we elaborate on this specific case to illustrate the methodology of ascertaining the recoverability and absolute amplitude calibration of impressed non-random signals.

The top right panel in Figure 7.1 is a dark subtracted image of a "typical" NCC OFF read. The horizontal striping results from the superposition of 60 Hz and 180 Hz EMI signals which are not NCC related. A 60 Hz signal repeats with a spatial frequency of 1588.815 pixel clock cycles, and a 180Hz signal three times more frequently. This gives vertical line spacings of these signals of ~ 12.22 and 4.07 rows. In this example the peak-to-peak amplitude of the 60/180Hz signal envelope is approximately 20 DN (see Figure 7.2, which is a row median over all pixels in one quad). Here, for illustrative purposes, the amplitude of the synthesized noiseless 6530 Hz signal was chosen to be equal to the measured envelope amplitude of the 60/180 Hz EMI signal..
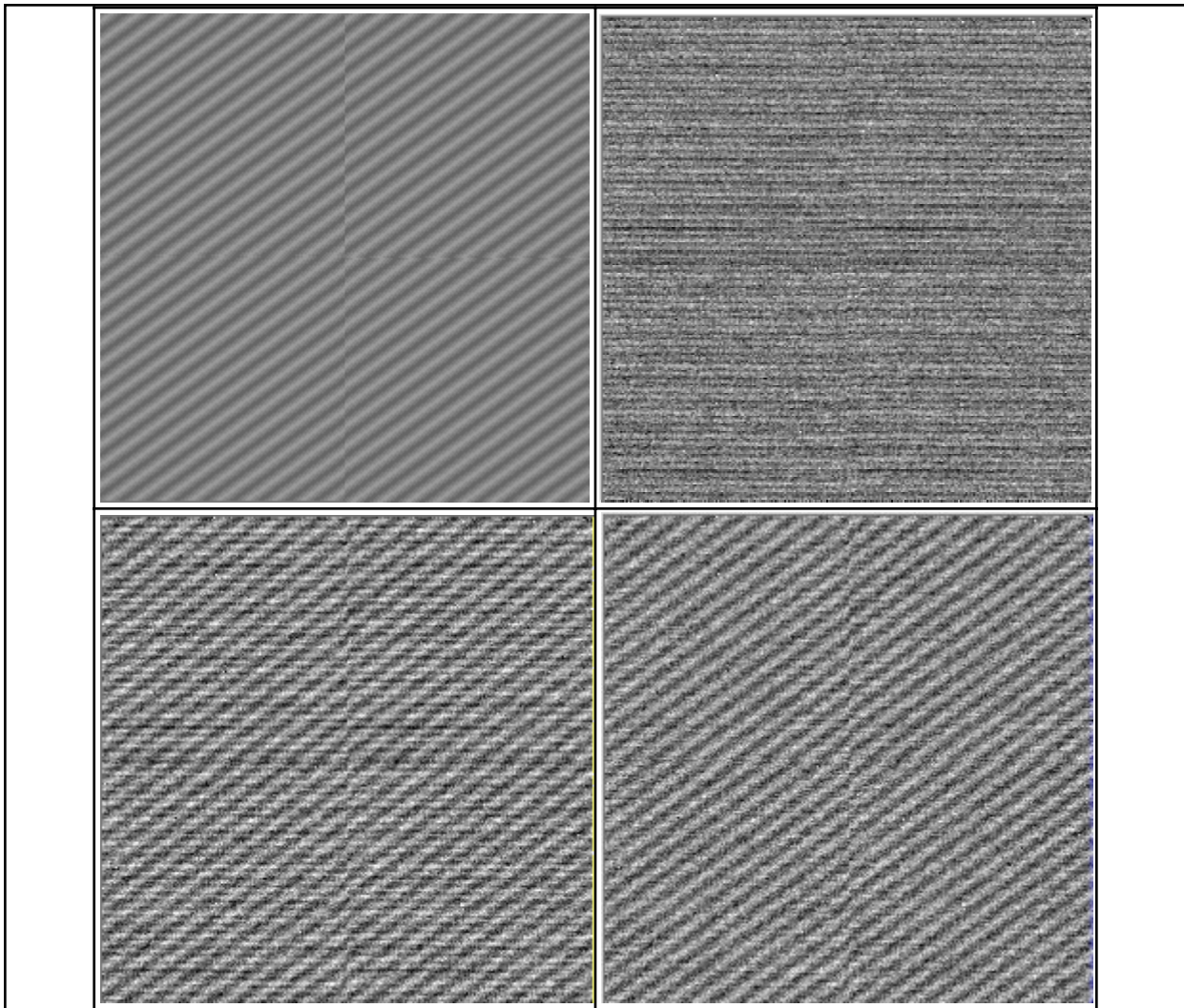
Figure 7.1 . Top Left - A 6530 Hz, +/- 10 DN (peak-to-peak) sinusoidal signal as sampled in a noiseless NICMOS image. Top Right - A typical observed NCC OFF dark-subtracted readout image, exhibiting 60Hz and 180Hz environmentally induced (non-NCC) noise. Bottom Left - Injection (coaddition) synthetic data into the observed frame. Bottom Right - Removal of the 60 and 180 Hz signals by row-median subtraction by quadrant.

Figure 7.2 . The ~ 10 DN peak-to-peak amplitude of the 60/180 Hz signal envelope is apparent in a plot of a row-wise median collapse of the affected image (see Fig 7.1,)
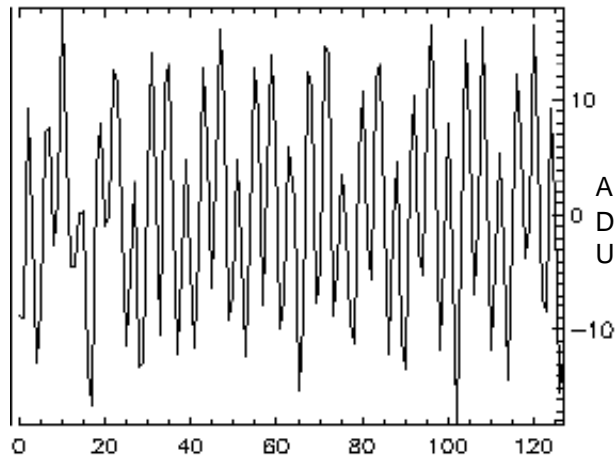
A power spectrum of the NCC OFF frame (Figure 7.1, top right), is shown in Figure 7.3 and clearly show the 60 and 180 Hz signals superimposed on a 1/f noise spectrum (which is a straight slanted line in this linear-log plot).
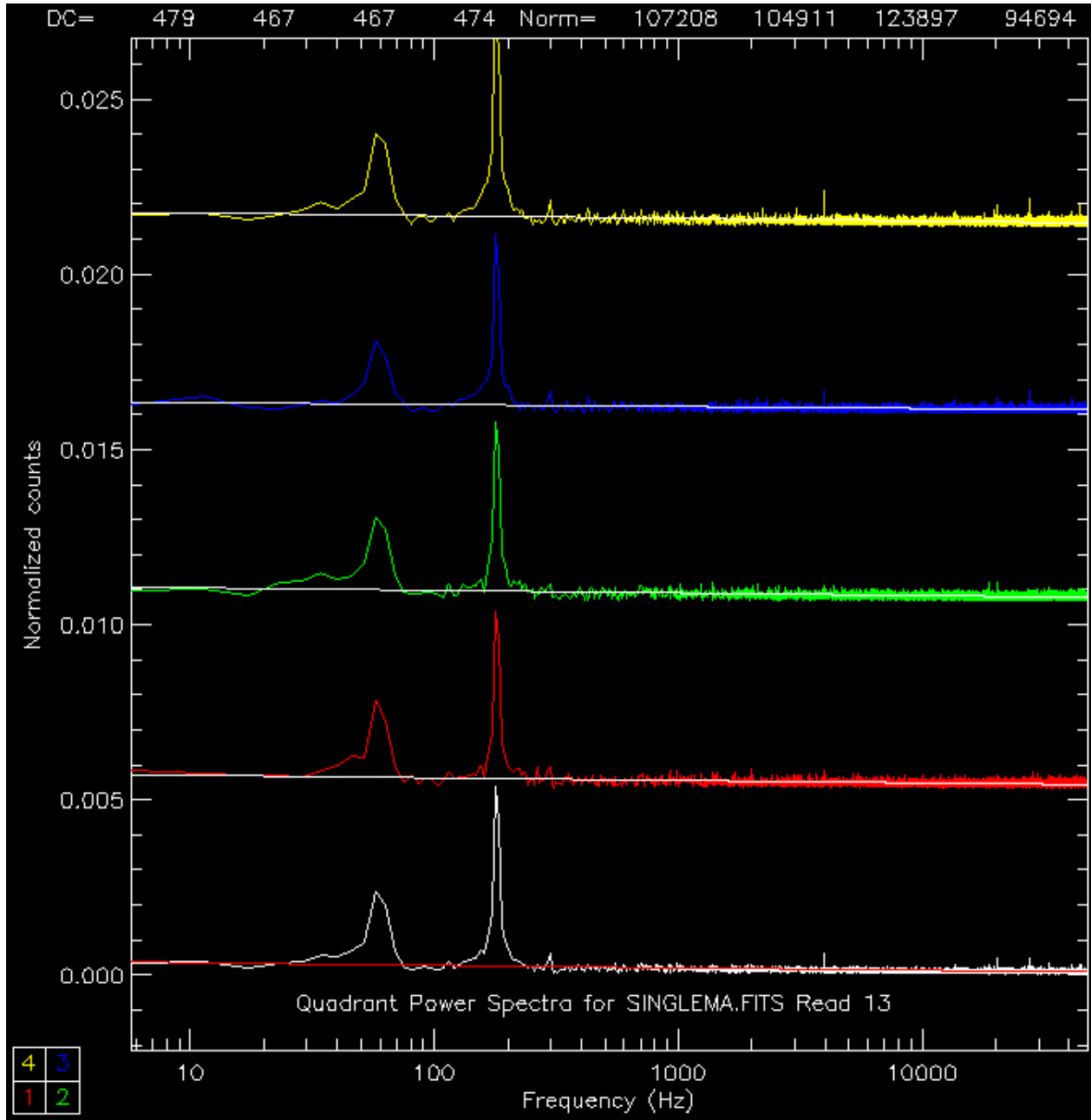
Figure 7.3 . Bottom (white) power spectrum of a typical NICMOS dark-subtracted readout with the NCC off. This spectrum is a mean of the spectra measured from each quadrant independently (see quadrant color key at lower left). Least squares fits to 1/f noise spectra are shown for each. The presence of 60 and 180 Hz environmental noise (and a 300 Hz harmonic) is obvious.

The red, green, yellow, and blue spectra were independently measured from data in quads 1, 2, 3, and 4, respectively. The white (bottom) spectrum is the average of the four spectra measured from each quad. The spectra are arbitrarily offset in the Y direction to aid in visibility. The dominant features are the 60Hz and 180Hz signals, though the 5th harmonic at 300 Hz is also easily seen. A few much lower amplitude monochromatic components at higher frequency are seen. Several of these appeared repeatedly throughout the test, such as at 3976, 20452 and 27608 Hz, but are environmental in origin. Perhaps they originate from the BRZ rack or other sources in the screen room. The measured 60 and 180Hz signals are not purely monochromatic, in part because the sampling is somewhat sparse at low frequency, but also because there is a slight asynchronicity in the 60 Hz line frequency both in the darks the reference files they were made from, and when

applied to individual reads in later observations. Thus the noise power in these bands are distributed in part to neighboring quantized frequency bins.

The statistical significance of the 1/f outliers in this spectrum may be assessed in Table 7.1 which gives an ordered list of the most significant deviations.

```
     TABLE 7.1 - Observed Frame Frequency Outliers
    > 3-sigma Outliers Sorted by maximum deviation
        Index      Frequency     Number STDEV
         31         177.596         56.4661
         32         183.325         45.6084
         10         57.2890         22.9922
         11         63.0179         18.2315
         30         171.867         16.8233
         33         189.054         12.1106
         29         166.138         8.00328
         34         194.783         7.76466
          9         51.5601         7.23818
        694         3975.86         5.18623
         35         200.511         4.97204
         27         154.680         4.92178
          8         45.8312         4.74131
       4819         27607.6         4.23643
         12         68.7468         4.02871
       3570         20452.2         3.98191
         28         160.409         3.94212
         52         297.903         3.89482


Coefficients for mean      0.000415432 -6.95607e-05
             for quad 1    0.000425958 -7.20409e-05
             for quad 2    0.000436875 -7.46133e-05
             for quad 3    0.000357034 -5.58012e-05
             for quad 4    0.000441853 -7.57863e-05
 number points exceeding   0.000271404 = 8
 in frequency range        5.72890 to 47658.7 Hz
 standard deviation        0.0000904682
```

Each frequency component which deviates from a least-squares fit to a 1/f spectrum by more than 3-sigma is given in this table. Additional information, beyond the scope of this report (but described in PSPECT documentation) to allow for scaling and intercomparing noise amplitudes in different spectra are also given. For example, the 180 Hz signal, measured discretely at 177.596 and 183.325 Hz, was found to be dominant in this spectrum. Note that in both these two "straddling" frequencies the 180 Hz signal component exceeds the 1/f spectrum by ~ 50 standard deviations. This is a completely unambiguous detection though the noise amplitude of the 60/180 Hz signal envelope is only about +/- 10 DN zero-to-peak (see Figure 7.3), which is also comparable to the per-pixel read-noise. This signal, however, is sampled by all 16K pixels in each quadrant, thereby improving the detectability by orders of magnitude.

This can now be compared to the same observed data, but with the synthesized, noiseless, 6350 Hz signal injected (as in the lower left image in Figure 7.1). The power spectrum of this composite image is shown in Figure 7.4
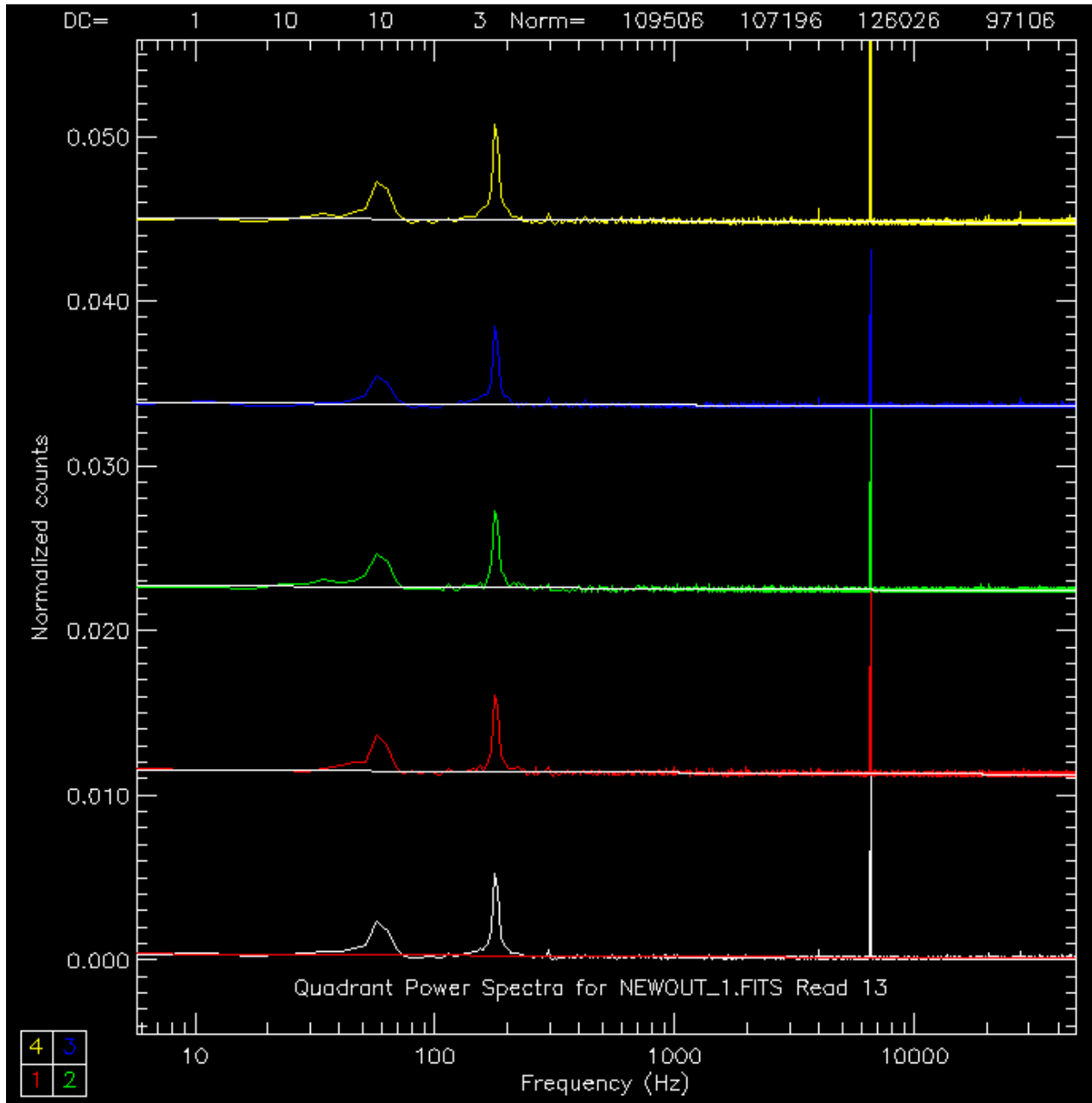

Figure 7.4. Power spectra of NCS OFF dark-subtracted frame with a 10 DN peak-to-peak sinusoidal signal injected. (Vertical axis is rescaled compared to figure 3.2 to accommodate peak of recovered signal).

The injected 6530 Hz sinusoidal signal had a peak-to-peak amplitude of +/- 10 DN. The amplitude dispersion of a sine function is 70.6% of the zero-to-peak amplitude, so in this case the injected 6530 Hz signal has a 1-sigma "noise" amplitude of 7 DN. The frame to which the synthetic data was added was taken immediately after the 180/0a read-noise assessment which had a 4-quad combined characteristic read-noise of 6.1 DN (32.7 electrons). Thus, the amplitude excursions in the injected signal were comparable to the quad-combined per-pixel read-noise.

Our injected sinusoid is sampled through 16384 pixels in each quad, so the measurement uncertainty from the read-noise for a periodic signal impressed on the aggregate of those pixels is

reduced by 128, or to 0.0428 DN, assuming all pixels are without defect. The tracer signal was recovered in the binned power spectrum peaking at 72 sigma above the 1/f noise measured from all pixels. Because of discrete sampling immediately adjacent frequency components of noise amplitudes 12.4 sigma (6525 Hz), 10 sigma (6536 Hz), and one bin further out 4.9 sigma (6519 Hz) and 3.8 sigma (6542 Hz) were found. The combined signal power amplitudes for all associated > 3-sigma 1/f outliers (see Table 7.2) implies an input signal of 5.2 DN, 17% lower than the injected signal.

```
TABLE 7.2 - Signal Implanted Frame Frequency Outliers
> 3-sigma Outliers Sorted by maximum deviation
           Index      Frequency     Number STDEV
           1140        6530.95        71.5528
             31        177.596        32.3159
             32        183.325        26.1098
             10        57.2890        13.0630
           1139        6525.22        12.4329
             11        63.0179        10.3995
           1141        6536.67         9.95075
             30        171.867         9.55250
             33        189.054         6.87774
           1138        6519.49         4.92385
             29        166.138         4.48863
             34        194.783         4.38262
              9        51.5601         4.01956
           1142        6542.40         3.82312
           1137        6513.76         3.31675
           1143        6548.13         3.01962


Coefficients for mean       0.000433554 -7.38308e-05
             for quad 1     0.000444121 -7.63205e-05
             for quad 2     0.000454858 -7.88505e-05
             for quad 3     0.000372564 -5.94602e-05
             for quad 4     0.000462685 -8.06946e-05
 number points exceeding   0.000462655 =          16
 in frequency range        5.72890 to      46925.4 Hz
 standard deviation   0.000154218
```

Similar small discrepancies were found in recovering injected signals impressed upon observed images spanning frequency ranges from 300 Hz to 30Khz and peak-to-peak signal amplitudes of 1 to 10 DN when injected into observed data containing significant levels of 60/180 Hz impressed pattern noise. This is primarily due to the fact that the global 1/f fits are slightly biased by the presence of the 60/180 Hz signals, as are the corresponding estimates of the 1-sigma dispersions in amplitudes about those fits. Thus, as a better estimator of the absolute amplitudes of the frequency components in the power spectrum, the implanted image was prewhitened in the spatial domain to remove (or significantly reduce) the 60/180 Hz signal. Since these signals change slowly with respect to the vertical pixel clock a row-collapsed median of each quadrant produces a model of this impressed combined signal which can then be subtracted from the image. This was done to produce the pre-whitened image in lower right panel of Figure 7.1. This is not perfect, as the phase relationship between the vertical clock and the impressed signals is not integral, but this is a sufficient approximation for this purpose. (One could prewhiten the data in the frequency domain by Fourier inversion, but this was not deemed necessary here). A power spectrum of the pre-whitened image is shown in Figure 7.5.
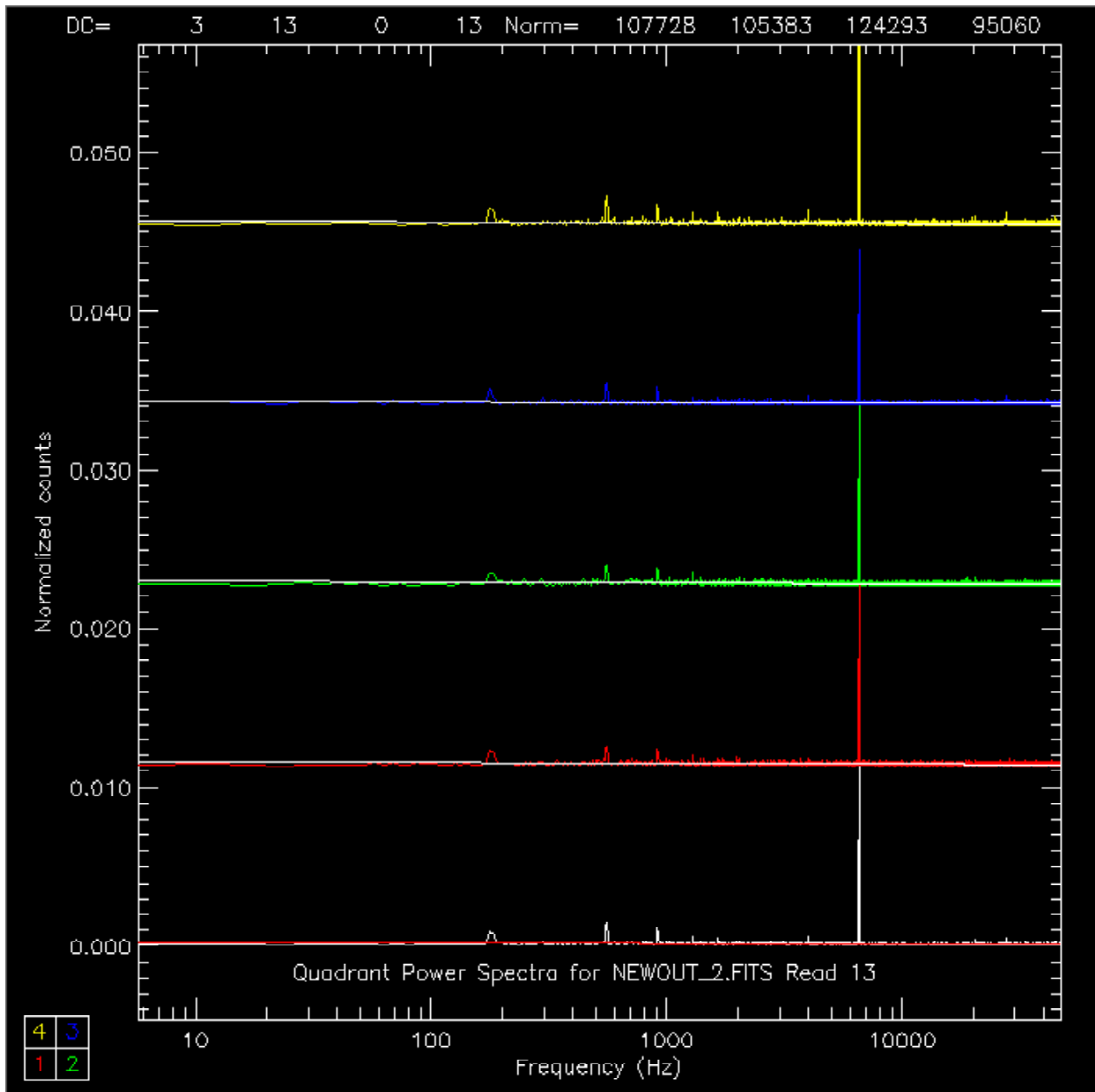
Figure 7.5 Power spectra of NCS OFF dark-subtracted frame with a 10 DN peak-to-peak sinusoidal signal injected, but pre-whitened to remove the 60/180Hz observed signal, in which the injected signal is fully recovered Signal removal by subtracting a row-median model in the spatial domain is imperfect leaving a small residual in the third harmonic a higher order spectrum of aliased frequencies.

The imperfection in this simple method of prewhitening manifests itself in an incomplete removal of the 180 Hz signature, and also in a low amplitude alias spectra toward higher frequencies, both of which may be seen in Figure 3.5. However, most of the power associated with these environmentally induced signals is removed, and with a better 1/f fit, and dispersion estimate, and the amplitude of the input signal can be better estimated from the power spectrum. The significant outliers in the prewhitened spectrum are listed in Table 7.3. In this prewhitened image the combined signal amplitudes for all > 3-sigma 1/f outliers associated with the 6530 Hz implanted signal implies an input signal gives 6.1 DN, in agreement with the input signal.

| TABLE 7.3 - Pre-Whitened Signal Implanted Frame |
| > 3-sigma Outliers Sorted by maximum deviation |

```
           Index      Frequency     Number STDEV
           1140        6530.95        82.8975
           1139        6525.22        14.5121
           1141        6536.67        11.5071
             97        555.703         9.42605
            159        910.895         7.17986
             96        549.974         6.74246
           1138        6519.49         5.81044
             31        177.596         5.38507
           1142        6542.40         4.66927
            160        916.624         4.46961
             32        183.325         4.18512
           1137        6513.76         3.94655
            225        1289.00         3.66640
           1143        6548.13         3.65050
            694        3975.86         3.54368
            224        1283.27         3.25397


    Coefficients for mean       0.000310285  -4.47861e-05
                 for quad 1     0.000324209  -4.80670e-05
                 for quad 2     0.000331188  -4.97115e-05
                 for quad 3     0.000273547  -3.61300e-05
                 for quad 4     0.000312191  -4.52353e-05
     number points exceeding    0.000406621 =            16
     in frequency range         5.72890 to       46925.4 Hz
     standard deviation     0.000135540
```

Discrepancies in injected and recovered signal amplitudes of a few tens of percent in un-prewhitened data were typical for data frames taken as part of this test. The magnitude of the discrepancy varied, as may be expected, as the amplitudes of the 60 and 180 Hz signals (which were not stable, through the two days of testing) also changed. To achieve an accurate absolute calibration of any induced EMI signals the 60 and 180 Hz environmental noise must first be removed.

8. ANALYSIS - METHODOLOGY

NCC/EMI induced signals impressed onto NICMOS science data readouts will adversely affect the image morphology in two significant ways. First, any band-limited periodic or quasi-periodic signals will result in herring-bone or video-pattern noise in the images arising from the interaction (beating and aliasing) between any such signals with the 10.49 microsecond horizontal and 1.3637 millisecond vertical pixel clocks. If such signals were of high enough noise amplitude they would be visible in images from which suitable dark reference frames were subtracted. We take advantage of the fact that since the time required to read through all 16,384 pixels (in each detector quadrant) is 174.5536 milliseconds (H=0.1745536s), so NCC induced signals with frequency components, F, in the likely range of concern would be sampled many times (FxH) in a single image readout. For example a 7200 Hz signal, corresponding to the likely on-orbit turbo-compressor rotation speed would be sampled 1257 times in a single science data readout. This greatly improves the signal visibility, by approximately root (FxH), providing very sensitive measures when the image is transformed into the temporal domain and the power spectra of the time-series evaluated. Second, any very broad-band, or "white" noise would alter the slope or random noise characteristics of the underlying detector's 1/f noise spectrum, which would also be sensitively measured, differentially, between NCC ON and NCS OFF frames. Finally, photodiodes multiplexed with the same base address but offset by 128 pixels in each quad are accessed simultaneously, but read out through different amplifiers and associated electronics. Thus, each quad provides an independent measure of induced signals which are spatially correlated in the four quads.

The structural characteristics of a raw images from NICMOS-3 detectors are complex owing to a number of intrinsic properties of the devices, and how they are controlled, accessed, and read-out. Fortunately, these artifacts (such as global and pixel-to-pixel gain variances, quadrant offsets, shading, amplifier glow, odd/even column striping, etc.) are very repeatable and stable and may be calibrated out of the raw readouts by subtracting well-matched dark reference files. Reference darks may be constructed from an assemblage of blanked-off multiaccum exposures clocked in exactly the same manner as the "target" exposures, with the detector at the same temperature. Combining same-reads in a stack of images by median combination, or if a sufficient number of images are taken by 3-sigma clipping to obviate quantization due to discrete 16-bit A-to-D conversion, produces the dark reference file. As this detector was not subjected to illumination in this test, we have no concerns about image persistence or related second order effects. Sets of "super-darks" were constructed from a dozen UA multiaccum sequences executed at the start and end of the test (on days 179 and 180, respectively) and were used as a fundamental reference. Interim darks, made from NCC OFF frames between periods cooler non-activity were used to assure the stability of the darks throughout the test.

Individual reads from each of the NCC ON and NCC OFF multiaccum sequences are dark subtracted. Power spectra of each quad is computed, and the simultaneously-sampled individual power spectra are averaged to further improve the sensitivity to impressed signals. The clocking of the NICMOS detector during its read-out cycle is such that each "row" of 128 pixels is overclocked by two cycles (20.98 microseconds) before the next row is read. This introduces a phase-offset in signals sampled between the last pixel read out in a row and the first pixel in the next row. To compensate for this, before computing the power spectrum of a quadrant, we pre-whiten the data very simply by inserting two samples between rows where the values of those samples are interpolated from adjacent pixels in time-sequential order. This demonstrably eliminates low-level side-lobes (and aliasing) which otherwise could affect the power spectra.

9. ANALYSIS - MECHANICS

To facilitate the analysis of large data sets of the nature obtained in this test, a special IDL based software package called PSPECT was created by the UofA NICMOS Project. PSPECT provides both a near-real time "quick-look" and bulk-processing capability for quantitatively evaluating the presence and levels of EMI induced noise in NICMOS multiaccum (or individual) images. PSPECT also allows for the construction and reduction of read-noise (RN) frames to serve as a basis for evaluating the system sensitivity. PSPECT was the primary S/W tool used in the analysis of the data from this test (augmented and cross-checked with IDP3, another IDL package developed by UofA, and Transform (a commercial package from RSI). The PSPECT S/W is available for download from the UofA/NICMOS anonymous ftp server (http://nicmos.as.arizona.edu), and may be used by others who wish to independently validate our results.

10. RESULTS - NO NOISE IS GOOD NOISE (or Much Ado About Nothing)

We have examined ALL readouts from NCC ON and OFF frames for evidence of any induced noise not seen in control (NCC OFF) frames taken as part of the same test sequences. We differentially evaluated a) raw reads , b) first-differenced raw reads, c) dark-subtracted reads and d) dark-subtracted first-differenced reads. Here we present a very small, but highly representative, sample of results obtained at several NCC operating speeds. We hasten to add that ALL data readouts throughout the test are essentially identical in their absence of NCC induced noise. The samples presented here are not particularly "good" or "bad", but are very typical and representative of the over-all test data.

Power spectra of five same-read dark-subtracted image frames are shown in Figure 10.1 for three images taken with the NCC running with turbo-compressor speeds of 5500, 6500 and 7200 RPS, and two frames with the NCC OFF just before and after these data were acquired. The reference dark used in the image subtractions was combined from 15 NCC OFF frames interleaved with periods of NCC operation from 179155504 to 179194305. and hence are contemporaneous with the image data. In this figure we arbitrarily chose read #2 for illustrative purposes, but again note that the results from all reads are statistically indistinguishable.

The 60/180 Hz environmental noise in the images from which the power spectra in Figure 10.1 were generated, have a peak-to-peak envelope intensities of ~ +/- 10 DN (see Figure 10.2, for example). The relative amplitude of the 60 Hz fundamental and its third harmonic, and the contribution to the total noise power by these frequency components remain fairly stable (as evidenced by the small sample in Figure 10.1) for the same reads in different multiaccums. They are somewhat different for different reads, which occur at different phases of a 60 Hz clock. We mention this only because, other than these obviously non-NCC related signals, all other aspects of all power spectra are identical to the level of sensitivity discussed in sections 6 and 7 whether the NCC is off, or running at different turbocompressor speeds.

A number of very sharp (monochromatic) peaks, other than higher order harmonics of the 60/180Hz components, are also seen at very low amplitude in the spectra. These occur repeatably, though in some cases intermittently, and with varying amplitudes, throughout the test and are attributed to sources other than the NCC (perhaps due to the BRZ itself). These components, which are most prevalent at 804, 4016 (fourth harmonic), 19616, 20417, 27648, 33273, 44050, and 45035 Hz, are also seen whether or not the NCC is running. Other than these, and a few other intermittent monochromatic peaks, also of non-NCC origin, no > 3-sigma departures from a 1/f spectrum are seen at any frequencies at any times. Note: As a basis for comparison, see Figures 3-5 of the April, 1998 test , where image contamination from NCC induced EMI was apparent.

In Figure 10.3 we show an examples of averaging power spectra obtained from each of the twenty-six reads in a multi-accum. In the UA multiaccum sequences, reads are spaced by 1.2 seconds, so the visibility of any periodic signals which persist over the 31.2 seconds of all 26 readouts will be enhanced. Quasi-stable signals may broaden as the overall S/N declines. The top panel in Figure 10.3 shows the averaging of the power spectra from the 26 reads of the same multiaccum from which read #2 was shown in Figure 10.1 with the NCC turbocompressor running at 7200 RPS.
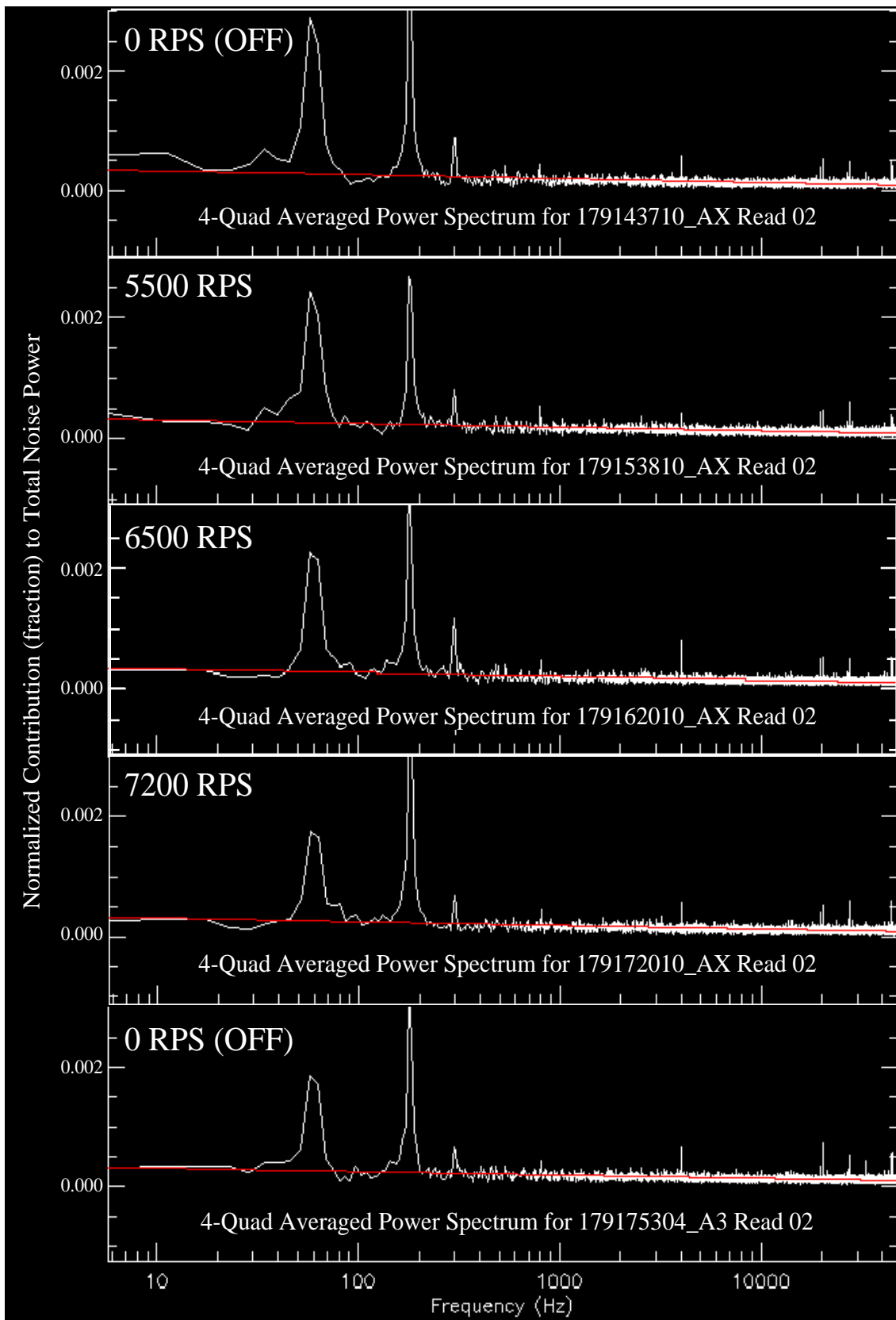
Figure 10.1. Four-quad averaged power spectra of contemporaneously dark-subtracted NICMOS-3 readouts with the NCC turbo-compressor running at three different speeds, and turned off as a comparative control.
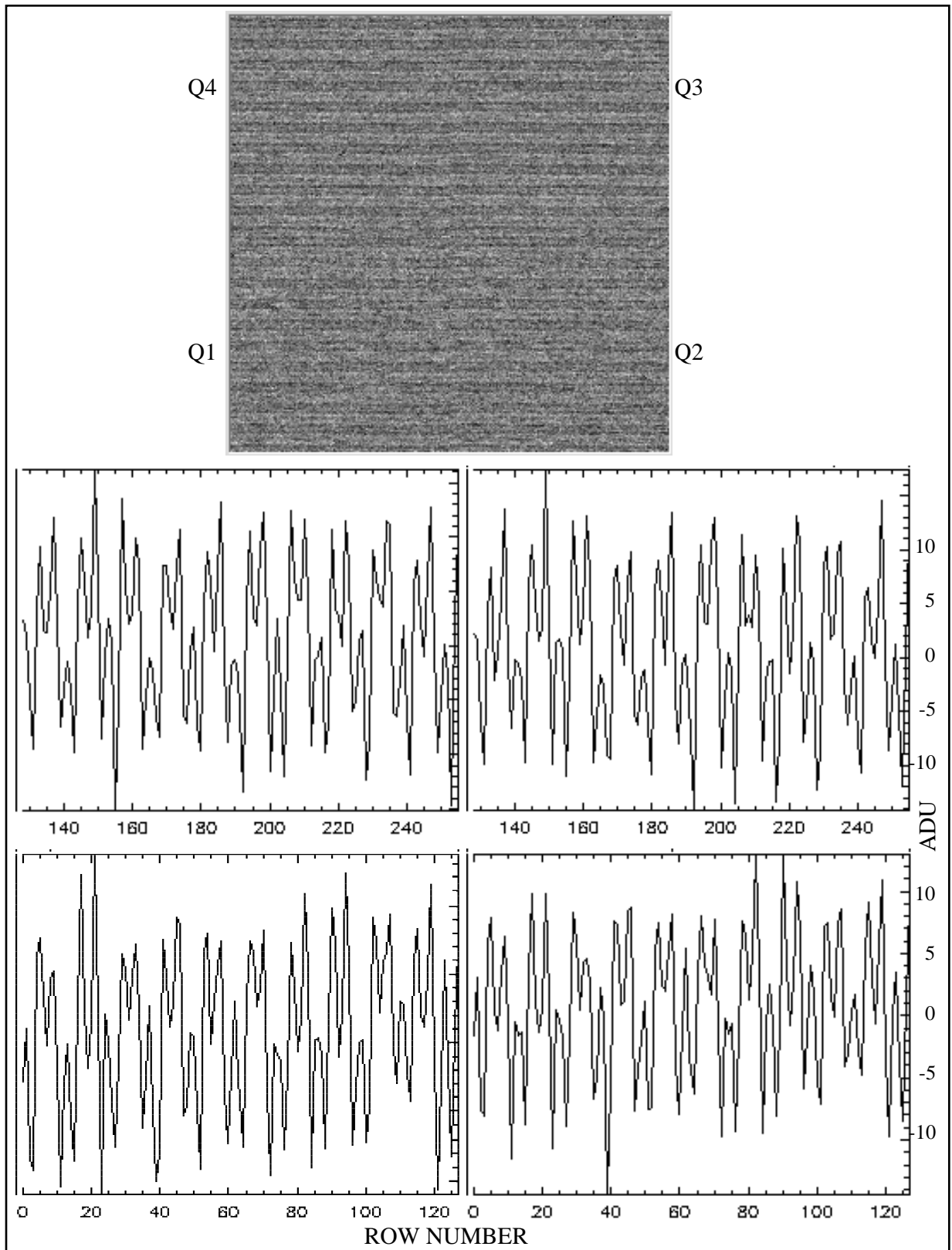
Figure 10.2. The 60/180Hz noise seen in the dark-subtracted images is typically represented by this NCC OFF frame, 179175304_A3, whose power spectrum is shown in Figure 10.1. Row-medians across each of the four detector quadrants (128x128 sub-arrays) below the image show the character and amplitude of the 60/180Hz signal.
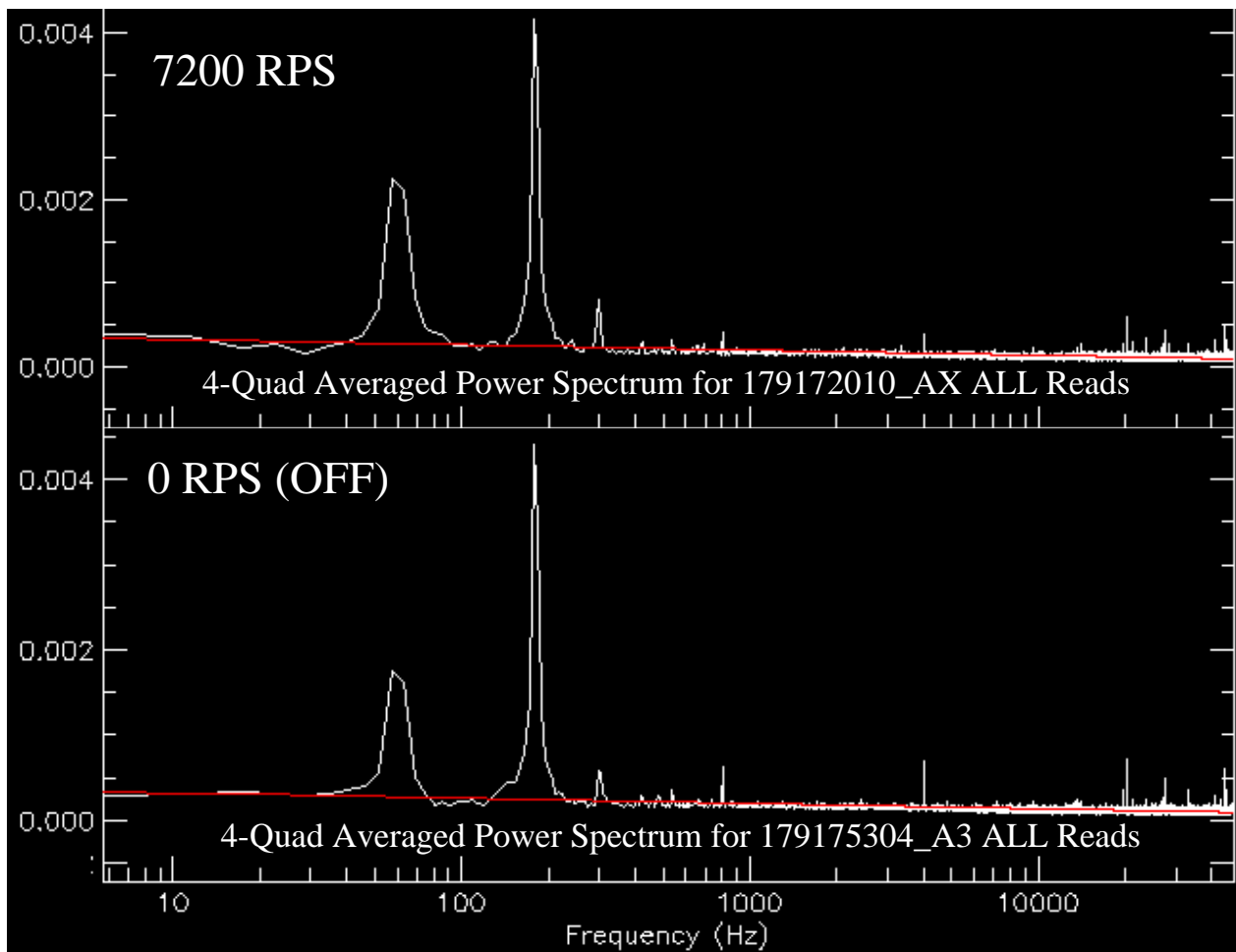
Figure 10.3. Similar to the bottom two panels in Figure 10.1, but the spectra presented here have been averaged from the 26 consecutive reads (each spaced by 1.2 seconds) obtained in the indicated multiaccum readouts. The improvement in S/N for temporally stable signals is readily apparent.

In the 26-read averaged power spectra the random 1/f noise due to the detector has been reduced in amplitude by root(26), and no NCC-induced signals are seen when compared to NCC OFF frames processed in the same manner (such as the one shown in the bottom panel of Figure 10.3). It is of interest to note that while some non-NCC signals increased in amplitude, no statistically significant signals associated with the NCC were seen. The same data are shown in Figure 10.4, but are cur-off below 500 Hz, and the plots rescaled (but not renormalized) vertically, to better show the lack of NCC-induced EMI in the presence of very low amplitude environmental EMI.
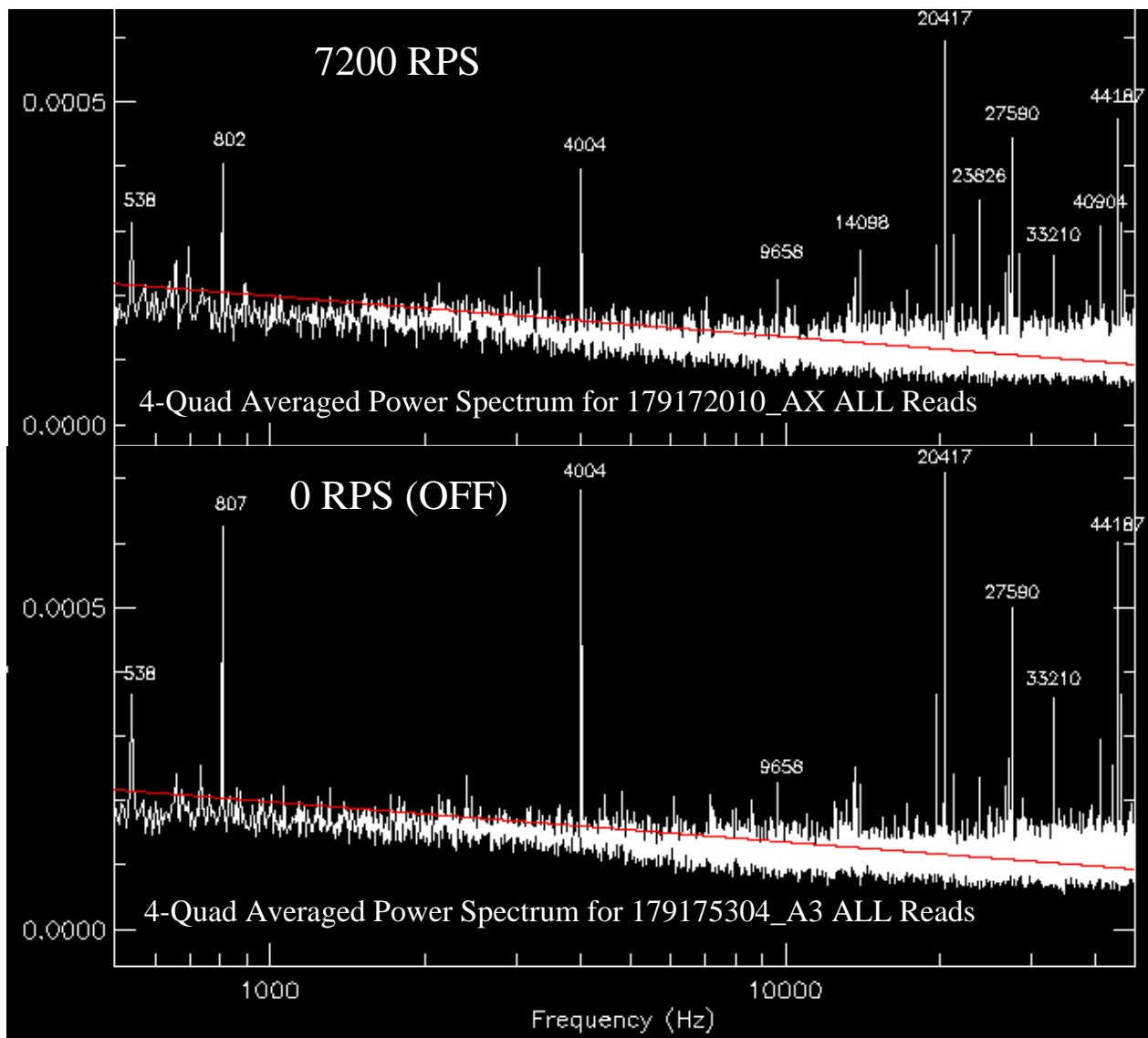
Figure 10.4. The lack of any NCC-induced signals sustained or broadened over ~ half a minute is typified in this pair very representative comparative power spectra (rescaled for better visibility) for frequencies > 500 Hz (~ 1% of the Nyquist cut-off).

11. CONCLUSIONS

Images obtained from a well-characterized NICMOS-3 flight spare detector, operated and read-out in a flight-like manner, were unaffected by the NCC. No EMI induced signals were seen any of more than 3000 NICMOS science data readouts analyzed with the NCC integrated to the NICMOS-3 test dewar with flight-like ground connections. Image data obtained with the NCC running at a variety of turbo-compressor speeds from 5,000 to 7,200 rps were identical to and indistinguishable from data acquired with the compressor idle, or the NCC turned off. The levels of sensitivity achieved in the test environment were comparable to those which were experienced on-orbit with the flight instrument during HST cycle 7. Science data readouts were examined in the spatial domain where periodic or quasi-periodic NCC induced EMI would have been evidenced as "pattern" or "herringbone" noise or, if broad-band, would have increased the dispersion in the pixel-to-pixel read noise. No such affects were seen. Readouts were also evaluated in the ~ 5 Hz to 50 Khz frequency domain (corresponding to spatial frequencies of a detector quadrant to pixel scales). No statistically significant deviations from a 1/f spectrum were found which could not be attributed to environmental signals (i.e., deviations were seen but were clearly not due to the NCC).

Based upon our analysis of the test data, as previously described, it is the opinion of the UofA test team that NICMOS on-orbit should be blind to the operation of the NCC from the purview of signals induced by electro-magnetic interference. This conclusion is predicated upon the assumption that the conducted and radiated emission paths established in integrating our test dewar with the NCC faithfully replicate the on-orbit configuration with high fidelity. We defer to the cognizant HST systems engineers at GSFC to validate that assumption. However, based upon ground-strap conducatances and radiated current probe measurements we believe this assumption is valid. If there are no further significant design or implementation changes in the NCC and its associated control electronics we believe this test unequivocally puts concerns for NCC/EMI contaminated NICMOS images behind us. We therefore look forward to the resumption of NICMOS science in HST Cycle 11 expecting no impact to the instrument's read-noise performance using this active cooling system in place of the now-depleted passive solid Nitrogen cryogen.

APPENDIX A - UofA NICMOS Project NCC/EMI Test Team

Glenn Schneider, Test Lead (On Site)

Pete Hubbard, Senior Electronics and Test Ssystem Engineer (On Site)

Tony Ferro, Computer Systems and Data Flow Manager (On Site)

Earl O'Neil, Analysis S/W Programming and Support

Betty Stobie, S/W Lead

Irene Barg, Data Archiving and Distribution

Note: This report is available electronically at the NICMOS Project UofA information server at:

http://nicmosis.as.arizona.edu:8000/NCC_EMI_2000/EMI2000.html

All inquirteies regarding this report, or requests for test data, should be directed to Glenn Schneider.

APPENDIX B - READ-NOISE STATISTICS

```
                    Read-Noise Statistics for 179/0a
            ALL Quads   Quad #1     Quad #2     Quad #3     Quad #4
Mean            11.563     13.593      13.302       9.667       9.679
Variance        52.575     22.535       3.338     167.642      85.094
Std Deviation    7.251      4.747       1.827      12.948       9.225
Clipped Mean    11.488     13.515      13.291       9.462       9.570
Clipped SDV      2.524      1.855       1.782       1.466       1.425
Bad Pixels      25          8          46           9          14
Total       757797     222704      217933      158378      317156
Median          11.22      13.48       13.27        9.41        9.52
Minimum          0.00       0.00        6.39        0.00        0.00
Maximum       1159.40     393.76       40.36     1159.40     1159.40
```

```
                    Read-Noise Statistics for 179/0d
            ALL Quads   Quad #1     Quad #2     Quad #3     Quad #4
Mean            11.181     12.602      12.372       9.899       9.876
Variance        65.604     20.203       2.975     230.055     116.200
Std Deviation    8.100      4.495       1.725      15.168      10.780
Clipped Mean    11.104     12.535      12.364       9.667       9.755
Clipped STDEV    2.062      1.714       1.675       1.456       1.407
Bad Pixels      22          9          40           9          12
Total       732787     206466      202704      162190      323611
Median          10.94      12.52       12.36        9.63        9.73
Minimum          0.00       0.00        6.18        0.00        0.00
Maximum       1397.55     435.27       51.87     1397.55     1397.55
```

```
                    Read-Noise Statistics for 179/0e
            ALL Quads   Quad #1     Quad #2     Quad #3     Quad #4
Mean            11.056     12.467      12.231       9.784       9.763
Variance        58.380     16.029       2.804     205.665     103.989
Std Deviation    7.641      4.004       1.675      14.341      10.197
Clipped Mean    10.979     12.406      12.224       9.556       9.643
Clipped SDV      2.031      1.685       1.642       1.434       1.373
Bad Pixels      25         11          38          10          15
Total       724590     204266      200396      160296      319926
Median          10.82      12.38       12.20        9.53        9.62
Minimum          0.00       0.00        5.34        0.00        0.00
Maximum       1207.77     343.95       35.14     1207.77     1207.77
```

```
                    Read-Noise Statistics for 180/0a
            ALL Quads   Quad #1     Quad #2     Quad #3     Quad #4
Mean            12.181     14.239      13.951      10.246      10.268
Variance        37.876     16.179       3.634     114.498      58.505
Std Deviation    6.154      4.022       1.906      10.700       7.649
Clipped Mean    12.121     14.181      13.940      10.078      10.177
Clipped SDV      2.587      1.928       1.870       1.500       1.469
Bad Pixels      27         10          44          11          17
Total       798326     233285      228572      167875      336465
Median          11.85      14.15       13.91       10.04       10.14
Minimum          0.00       0.00        7.37        0.00        0.00
Maximum       1191.57     304.60       33.32     1191.57     1191.57
```

```
                 Read-Noise Statistics for 180/0b
            ALL Quads   Quad #1    Quad #2    Quad #3    Quad #4
Mean            11.558     13.073     12.817     10.206     10.172
Variance        93.512     20.659      3.084    340.044    171.294
Std Deviation    9.670      4.545      1.756     18.440     13.088
Clipped Mean    11.476     13.001     12.811      9.960     10.043
Clipped SDV      2.166      1.780      1.725      1.587      1.477
Bad Pixels          20          9         39          8         11
Total           757488     214188     209999     167218     333304
Median           11.29      12.98      12.80       9.92      10.01
Minimum           0.00       0.00       6.34       0.00       0.00
Maximum        2031.30     374.96      35.20    2031.30    2031.30


                 Read-Noise Statistics for 180/0c
            ALL Quads   Quad #1    Quad #2    Quad #3    Quad #4
Mean            11.503     13.008     12.759     10.134     10.123
Variance        55.300     22.556      3.114    185.350     93.942
Std Deviation    7.436      4.749      1.765     13.614      9.692
Clipped Mean    11.427     12.933     12.749      9.922     10.010
Clipped SDV      2.144      1.775      1.723      1.520      1.448
Bad Pixels          25          9         40          8         13
Total           753866     213120     209043     166038     331708
Median           11.26      12.90      12.74       9.88       9.97
Minimum           0.00       0.00       6.09       0.00       0.00
Maximum        1024.64     443.74      42.15    1024.64    1024.64


                 Read-Noise Statistics for 180/0d
            ALL Quads   Quad #1    Quad #2    Quad #3    Quad #4
Mean            11.451     12.944     12.705     10.084     10.078
Variance        42.243     17.136      3.042    138.920     70.613
Std Deviation    6.499      4.140      1.744     11.786      8.403
Clipped Mean    11.384     12.879     12.699      9.897      9.980
Clipped SDEV     2.115      1.757      1.706      1.427      1.401
Bad Pixels          27         13         46         10         14
Total           750457     212079     208152     165211     330227
Median           11.20      12.86      12.70       9.88       9.96
Minimum           0.00       0.00       6.03       0.00       0.00
Maximum        1095.99     342.39      35.82    1095.99    1095.99


                 Read-Noise Statistics for 180/0e
            ALL Quads   Quad #1    Quad #2    Quad #3    Quad #4
Mean            11.379     12.866     12.626     10.017     10.012
Variance        41.247     22.894      3.015    129.280     65.789
Std Deviation    6.422      4.785      1.736     11.370      8.111
Clipped Mean    11.312     12.790     12.617      9.833      9.916
Clipped SDEV     2.114      1.758      1.694      1.435      1.420
Bad Pixels          24          8         53         11         14
Total           745742     210801     206868     164110     328072
Median           11.14      12.76      12.58       9.79       9.87
Minimum           0.00       0.00       5.82       0.00       0.00
Maximum        1170.94     407.22      36.77    1170.94    1170.94
```